Effective potential of the Polyakov loop in the Hamiltonian approach to QCD

Markus Quandt and Hugo Reinhardt

Institute for Theoretical Physics, University of Tübingen,
Auf der Morgenstelle 14, D-72076 Tübingen, Germany

We investigate the effective potential of the Polyakov loop, which is the order parameter for the deconfinement phase transition in finite temperature QCD. Our work is based on the Hamiltonian approach in Coulomb gauge where finite temperature T is introduced by compactifying one space direction. We briefly review this approach and extend earlier work in the Yang-Mills sector by including dynamical quarks. In a first approximation, we follow the usual functional approach and include only 1-loop contributions to the energy, with the finite temperature propagators replaced by their $T = 0$ counterparts. It is found that this gives a poor description of the phase transition, in particular for the case of full QCD with $N_f = 3$ light flavors. The physical reasons for this unexpected result are discussed, and pinned down to a relative weakness of gluon confinement compared to the deconfining tendency of the quarks. We attempt to overcome this issue by including the relevant gluon contributions from the 2-loop terms to the energy. We find that the 2-loop corrections have indeed a tendency to strengthen the gluon confinement and weaken the unphysical effects in the confining phase, while slightly increasing the (pseudo)critical temperature T^* at the same time. To fully suppress artifacts in the confining phase, we must tune the parameters to rather large values, increasing the critical temperature to $T^* \approx 340$ MeV for $G = SU(2)$.

I. INTRODUCTION

A detailed understanding of strongly interacting matter under extreme conditions (i.e. high temperatures or baryon densities) is among the most challenging and actively studied problems in particle physics today. While experimental studies in particular at the Large Hadron Collider are now starting to probe into the physics of the quark gluon plasma, the theoretical description of this topic amounts to a detailed computation of the phase diagram of quantum chromodynamics (QCD) [1,2]. Lattice calculations allow for precise *ab initio* studies at nonzero temperatures and vanishing baryon density, while Monte Carlo simulations at nonzero baryon density are hampered by the so-called *sign problem* [1,3]. Several methods have been put forward to address this shortcoming, but so far they all seem to be restricted to rather small chemical potentials. The most promising techniques to overcome this problem are, at the time of this writing, the nonperturbative continuum approaches known as functional methods. Such tools have therefore become an important part of the theoretical study

of QCD under extreme conditions, using techniques such as Dyson-Schwinger equations (DSEs) [4], functional renormalization group (FRG) flow equations [5], covariant variational methods [6], or semiphenomenological approaches based on a massive gluon propagator [7,8]. One particularly transparent method is the so-called *Hamiltonian approach* to QCD in Coulomb gauge [9], which is based on a variational determination of the QCD ground state wave functional; for a recent review see Ref. [10].

QCD has a rich phase structure that can be described by the partition function depending on temperature and chemical potential (i.e. baryon density). Virtually all visible matter in the Universe is in the hadronic phase, though different phases of QCD may be realized at extremely high densities e.g. in the core of neutron stars [11,12]. The hadronic phase is characterized by permanent color confinement and the spontaneous breaking of chiral symmetry. For the latter, a suitable order parameter is the chiral quark condensate, while deconfinement is described, at least in the absence of dynamical quarks, as a transition from a center symmetric phase at low temperatures to a high temperature phase with center symmetry broken [13,14]. Any quantity that transforms nontrivially under center transformations can thus serve as an order parameter for confinement in pure Yang-Mills theory. A particularly transparent picture emerges in the imaginary time formalism, where finite temperature is introduced by Wick

rotating to Euclidean space and compactifying the Euclidean time direction to a circle of circumference $\beta = 1/T$. Then the Polyakov loop[1]

$$\mathsf{L}(\boldsymbol{x}) \equiv \frac{1}{N} \mathrm{tr} \mathcal{P} \exp\left[-\int_0^\beta dx_0 A_0(x_0, \boldsymbol{x})\right] \qquad (1)$$

transforms as $\mathsf{L}(\boldsymbol{x}) \to z\mathsf{L}(\boldsymbol{x})$ under a center transformation with $z \in Z(N)$, and hence $\langle \mathsf{L}(\boldsymbol{x}) \rangle = 0$ in the center symmetric (confined) phase, while $\langle \mathsf{L}(\boldsymbol{x}) \rangle \neq 0$ in the center broken (deconfined) phase. The connection between center symmetry and color confinement comes from the formal identity

$$\langle \mathsf{L}(\boldsymbol{x}) \rangle = \exp\left[-\beta F_\beta(\boldsymbol{x})\right], \qquad (2)$$

which relates the Polyakov loop to the free energy $F_\beta(\boldsymbol{x})$ of a single quark immersed in the thermal QCD background. It must be emphasized that this relation is formal, since a single color charge in the fundamental representation cannot be screened by gluons, i.e. the overlap of states from the vacuum sector with single static quark states must vanish. This is a consequence of Gauss' law and has nothing to do with confinement. In particular, it does not mean that the Eq. (2) cannot be computed or has to vanish—it merely indicates that $\mathsf{L}(\boldsymbol{x})$ cannot consistently represent a single static quark and the usual identification Eq. (2) is a shortcut: the true interpretation relies on the correlator $\langle \mathsf{L}(\boldsymbol{x}) \cdot \mathsf{L}(\boldsymbol{y})^* \rangle = \exp(-\beta V(r))$, which describes the interaction energy $V(r)$ of a static quark-antiquark pair at distance $r = |\boldsymbol{x} - \boldsymbol{y}|$. Cluster decomposition then leads to $V(\infty) = \infty$ *iff* $\langle \mathsf{L} \rangle = 0$, i.e. confinement in the center symmetric phase; a similar reasoning applies to deconfinement in the center broken phase.

The Polyakov loop $\mathsf{L}(\boldsymbol{x})$ is a rather complicated quantity in continuum approaches, mainly because of path ordering. A convenient way to circumvent this problem is to go to Polyakov gauge,

$$\partial_0 A_0^{b_0} = 0, \qquad A_0^{\bar{b}} = 0, \qquad (3)$$

where $\{T^{b_0}\}$ are the generators of the Cartan subgroup H, while the remaining generators $\{T^{\bar{b}}\}$ span the coset G/H of the color group $G = SU(N)$. In this gauge, the Polyakov loop requires no path ordering,

$$\mathsf{L}(\boldsymbol{x}) = \frac{1}{N} \mathrm{tr} \exp\left[-\beta A_0^{b_0} T^{b_0}\right]. \qquad (4)$$

Furthermore, it was argued in Refs. [5,15] that not only the Polyakov loop, but also the simpler quantity $\langle A_0 \rangle$ can serve as an order parameter for confinement in this gauge. This

statement was originally proved for $G = SU(2)$ using Jensen's inequality, but since then has also been shown to generalize to $G = SU(3)$ [16] and, using different techniques, to an even larger class of compact color groups [7].

For most continuum studies, it is more convenient to work in *background gauge*, where an external background field a_μ is split off the gauge field, $A_\mu = \mathsf{a}_\mu + Q_\mu$, and the quantum field Q is subject to the condition

$$[D_\mu[\mathsf{a}], Q_\mu] = 0, \qquad (5)$$

where $D_\mu[A] \equiv \partial_\mu + A_\mu$ is the covariant derivative. This has the benefit that the effective action $\Gamma_\mathsf{a}[Q]$ of the fluctuation field Q_μ is a gauge-invariant functional of a at $Q = 0$. If the background field $\mathsf{a}_\mu = \delta_{\mu 0} \mathsf{a}_0$ itself is taken spatially constant and in Polyakov gauge,

$$\partial_0 \mathsf{a}_0^{b_0} = 0, \qquad \mathsf{a}_0^{\bar{b}} = 0, \qquad (6)$$

this entails that the main contribution to Γ_a is the Polyakov loop L, which is the only gauge invariant quantity that can be formed from such an a_0. Fluctuations may also involve further degrees of freedom but it has been argued [5,15] that gauge invariant features such as the location and order of the phase transition can also be extracted from the effective action of the background field a_0. This statement has since been confirmed by lattice simulations and numerous continuum studies, cf. below. We will also adopt this procedure in the following and understand the effective potential of the Polyakov loop as the effective potential of a background field obeying Eq. (6), though the two quantities are, in principle, distinct [5].

It should be mentioned that the background effective action is $\Gamma_a[Q = 0] = \Gamma[\mathsf{a}]$, where $\Gamma[A]$ is the usual effective action for the full gauge field A, taken in the somewhat unusual gauge $[D_\mu[\mathsf{a}], A_\mu - \mathsf{a}_\mu] = 0$. The background field a_0 thus plays a twofold role both as the argument of Γ and the parameter in the gauge condition defining it. For most values of a_0, the effective action $\Gamma[\mathsf{a}_0]$ will not be *manifestly* center symmetric. This is not an issue if the theory is treated exactly, but approximations are more likely to break center symmetry and obscure the confinement mechanism. To overcome this issue, it was proposed in Ref. [8] to separate these two roles of the background field and take the background in the gauge condition such that center symmetry is manifest. We have not adopted this formulation in the present work and rather checked center symmetry *a posteriori*: As detailed later, the pure gauge effective potentials computed in the present formulation are always center symmetric in both the confined and deconfined phases, and the breaking occurs spontaneously through the location of the minimum, or explicitly in the presence of quarks.

The Polyakov loop is no longer a strict order parameter once dynamical quarks are included, and lattice

---

[1]Here and in the following, N denotes the number of colors in the gauge symmetry group $SU(N)$, and $\mathcal{P}$ indicates path ordering.

calculations indicate that the finite temperature phase transition in pure Yang-Mills theory turns into an analytic crossover at a significantly lower pseudocritical temperature, which depends on the exact observable used in its definition (see [17] for details and recent numerical results). This agrees also with findings in random matrix models [18]. As explained above, most functional methods employ the background field a_0 in Polyakov gauge as an order parameter for the pure Yang-Mills case. We will continue to use this scheme also in full QCD, even though a_0 is no longer a strict order parameter and the results may differ from lattice studies made with other pseudo order parameters.

The Hamiltonian approach employed in this paper works in Coulomb gauge and thus exhibits only physical (transversal) degrees of freedom. This is not only beneficial for *Ansätze* of the trial wave functionals, but it also avoids the emergence of unphysical (longitudinal or ghost) particles which dominate the vacuum in other functional approaches. The method is very efficient in computing vacuum properties, but the absence of ghost dominance leads to a gluon confinement which is much more fragile as compared to other functional techniques. This becomes apparent when dynamical quarks are introduced, and we attempt to overcome this issue in the present paper by adjusting renormalization constants and, in particular, including higher loop orders.

The study of the Polyakov loop in the Hamilton approach is, at first, hampered by the fact that the fields live in three-dimensional position space and no Euclidean time is available. Finite temperature must therefore be introduced in real time using the full set of thermal states instead of studying vacuum properties [19]. In addition, the method necessarily works in Weyl gauge, $A_0 = 0$, which also prevents us from studying the Polyakov loop directly. These issues were overcome in Ref. [20], where the full Euclidean $O(4)$ symmetry of the underlying theory was used to introduce a heat bath via compactification of one *spatial* axis, say the 3-direction. Finite temperature calculations then involve the study of the ground state properties on the semicompactified spatial manifold $\mathbb{R}^2 \times S^1(\beta)$, and the Polyakov loop winds around the compactified spatial direction instead of the Euclidean time. This setting has been used successfully to compute the deconfinement phase transition in pure Yang-Mills theory [21–23]. In the present study, we extend these calculations to full QCD including dynamical quarks.

This paper is organized as follows: In the next section, we review the techniques required to formulate the Hamiltonian approach in background gauge and at finite temperatures. The renormalization at the 1-loop level is described in Sec. III, which also presents details on our numerical methods and the variational kernels used. In Sec. IV, the numerical results for the Polyakov loop at 1-loop level are presented and discussed. We find that the

transition region is described well, but the numbers do *not* represent the confining phase accurately at small temperatures once dynamical quarks are included. We attempt to resolve this issue by including the relevant parts of the 2-loop contribution in Sec. V. There is a residual parameter dependency due to our incomplete renormalization at this order, and we discuss the parameter range in which the 2-loop contribution proves to be beneficial. The paper is concluded in Sec. VI with a discussion of our findings and an outlook to further improvements.

II. HAMILTONIAN APPROACH TO QCD IN THE BACKGROUND GAUGE

For pure Yang-Mills theory, the background field method in the Hamiltonian approach was discussed in detail in Ref. [22]. For completeness and to fix our notation, we summarize the essential features and then discuss the extension to the quark sector.

A. The Hamiltonian in background gauge

The canonical quantization of QCD in Weyl gauge $A_0 = 0$ results in the Hamiltonian

$$H = H_{\text{YM}} + H_q. \tag{7}$$

Here, the gluon contribution reads

$$H_{\text{YM}} = \frac{1}{2} \int d^3x \left[g^2 \mathbf{\Pi}^2(\boldsymbol{x}) + \frac{1}{g^2} \boldsymbol{B}^2(\mathbf{x}) \right] \tag{8}$$

and involves, besides the conjugate momentum operator $\Pi_k = -i\delta/\delta A_k$ and the coupling strength g, also the color magnetic field $\boldsymbol{B}^a = \boldsymbol{\nabla} \times \boldsymbol{A}^a + \frac{1}{2} f^{abc} \boldsymbol{A}^b \times \boldsymbol{A}^c$. The quark sector is simply the usual Dirac Hamiltonian of a massive fermion (with the standard 4×4 matrices α and β) coupled covariantly $(\boldsymbol{D}(\boldsymbol{x}) = \boldsymbol{\nabla} + \boldsymbol{A}(\boldsymbol{x}))$ to the gluons,

$$H_q = \int d^3x \, \psi^\dagger(\boldsymbol{x})[\boldsymbol{\alpha} \cdot \boldsymbol{D}(\boldsymbol{x}) + \beta m]\psi(\boldsymbol{x}). \tag{9}$$

At this point, the residual gauge symmetry of time-independent gauge transformation has not yet been fixed. This is reflected by the existence of a time-independent constraint (Gauss' law),

$$\hat{\boldsymbol{D}} \cdot \mathbf{\Pi}|\Phi\rangle = \rho|\Phi\rangle, \tag{10}$$

where the hat denotes the adjoint color representation,

$$\hat{D}_k^{ab} = \hat{\partial}_k^{ab} + \hat{A}_k^{ab} = \delta^{ab}\partial_k - f^{abc}A_k^c,$$

and $\rho^a(\boldsymbol{x}) = -i\psi^\dagger(\boldsymbol{x})T^a\psi(\boldsymbol{x})$ is the color charge density of the quarks. We must resolve Gauss' law explicitly in

background gauge. To this end, we first introduce generalized longitudinal and transversal projectors,

$$\hat{\ell}_{ik} = \hat{\mathsf{d}}_k [\hat{\mathsf{d}} \cdot \hat{\mathsf{d}}]^{-1} \hat{\mathsf{d}}_k, \qquad \hat{t}_{ik} = \hat{\delta}_{ik} - \hat{\ell}_{ik}, \qquad (\hat{\delta}_{ik}^{ab} = \delta^{ab} \delta_{ik}), \tag{11}$$

where $\hat{\mathsf{d}} = \hat{\partial} + \hat{\mathsf{a}}$ is the covariant derivative of the background field. For a constant background field a in the Cartan subalgebra, we have $[\hat{\mathsf{d}}_i, \hat{\mathsf{d}}_k] = 0$ and the generalized projectors enjoy the same properties as the ordinary projectors.

We can now follow the resolution of Gauss' law in analogy to the standard derivation of the gauge fixed Hamiltonian in Coulomb gauge. The result is the background gauge-fixed QCD Hamiltonian,

$$H_{\text{fix}} = H_{\text{YM}}^{\perp} + H_q + H_C, \tag{12}$$

in which all (background) longitudinal fields have been eliminated. To simplify the notation, we will therefore drop the superscript "$\perp$" on all fields and stipulate that $A = A^{\perp}$ and $\Pi = \Pi^{\perp}$ are background transversal in the sense of Eq. (11), unless stated otherwise. The quark section, H_q, remains unchanged and still reads as in Eq. (9). In the gluon contribution, however, the gauge fixing has introduced the Faddeev-Popov determinant of the background gauge

$$\mathcal{J}_{\mathsf{a}}[A] = \det[-\hat{\boldsymbol{D}} \cdot \mathsf{d}], \tag{13}$$

which enters the kinetic energy,

$$H_{\text{YM}} = \frac{g^2}{2} \int d^3x \, \mathcal{J}_{\mathsf{a}}^{-1}[A] \mathbf{\Pi}(\boldsymbol{x}) \cdot \mathcal{J}_{\mathsf{a}}[A] \mathbf{\Pi}(\boldsymbol{x}) + \frac{1}{2g^2} \int d^3x \, \boldsymbol{B}(\boldsymbol{x}) \cdot \boldsymbol{B}(\boldsymbol{x}). \tag{14}$$

In addition, a new non-Abelian color interaction emerges,

$$H_C = \frac{g^2}{2} \int d^3(x, y) \mathcal{J}_{\mathsf{a}}^{-1}[A] \rho_{\text{tot}}^a(\boldsymbol{x}) \mathcal{J}_{\mathsf{a}}[A] F^{ab}(\boldsymbol{x}, \boldsymbol{y}) \rho_{\text{tot}}^b, \tag{15}$$

where

$$\hat{F}^{ab}(\boldsymbol{x}, \boldsymbol{y}) = \int d^3z [(-\hat{\mathsf{d}} \cdot \hat{\boldsymbol{D}})^{-1}]^{ac}(\boldsymbol{x}, \boldsymbol{z}) [-\hat{\mathsf{d}} \cdot \hat{\mathsf{d}}]^{-1}(\boldsymbol{z}) \\ \times [(-\hat{\mathsf{d}} \cdot \hat{\boldsymbol{D}})^{-1}]^{cb}(\boldsymbol{z}, \boldsymbol{y}) \tag{16}$$

is the background gauge analog of the non-Abelian Coulomb term, which generalizes the Coulomb interaction in electrostatics. The total charge $\rho_{\text{tot}} = \rho_{\text{YM}} + \rho$ receives contributions from both the matter and the gauge fields; in particular, the gluon charge $\rho_{\text{YM}} = -\hat{\boldsymbol{D}} \mathbf{\Pi}$ simplifies to $\rho_{\text{YM}} = -(\hat{A} - \hat{\mathsf{a}}) \mathbf{\Pi}$ since $\mathbf{\Pi}$ is background transversal.

B. Trial wave functionals for full QCD

In the next step, we have to define trial wave functions $|\Phi\rangle$ which obey the constraint $\langle A \rangle_{\Phi} = \mathsf{a}$. We start with the wave functionals of the Hamiltonian approach in Coulomb gauge ($\mathsf{a} = 0$) [9,24], which employ a product *Ansatz* for the Yang-Mills and quark sector,

$$|\Phi[A]\rangle = \Phi_{\text{YM}}[A] |\Phi_q[A]\rangle. \tag{17}$$

The gluon part is a modified Gaussian type of functional,

$$\Phi_{\text{YM}}[A] = \mathcal{N} \cdot \mathcal{J}[A]^{-\frac{1}{2}} \cdot \mathcal{I}[A]^{-\frac{1}{2}} \cdot \tilde{\Phi}_{\text{YM}}[A], \tag{18}$$

$$\tilde{\Phi}_{\text{YM}}[A] = \exp\left(-\frac{1}{2g^2} \int d^3(x, y) A_i^a(\boldsymbol{x}) \omega(\boldsymbol{x} - \boldsymbol{y}) A_i^a(\boldsymbol{y})\right), \tag{19}$$

where ω is a variation kernel, and $\mathcal{N}$ is a normalization constant involving ω. The additional normalization $\mathcal{I}[A] = \langle \Phi_q | \Phi_q \rangle$ comes from the quark sector, for which a Slater determinant inspired by BCS theory will be used [9,24],

$$|\Phi_q[A]\rangle = \exp\left[-\int d^3(x, y) \psi_+^{m\dagger}(\boldsymbol{x}) K^{mn}(\boldsymbol{x}, \boldsymbol{y}) \psi_-^n(\boldsymbol{y})\right] |0\rangle. \tag{20}$$

Here $\psi_{\pm}$ are the positive/negative energy components of the fermion field, $|0\rangle$ is the bare fermionic vacuum (Dirac sea) and m, n are color indices in the fundamental representation. The variational kernel $K[A]$ may depend explicitly on the gluon field and can be decomposed in Dirac structures,

$$K^{mn}(\boldsymbol{x}, \boldsymbol{y}) = \beta S^{mn}(\boldsymbol{x}, \boldsymbol{y}) - i \int d^3z [V_b^{mn}(\boldsymbol{x}, \boldsymbol{y}; \boldsymbol{z}) + \beta W_b^{mn}(\boldsymbol{x}, \boldsymbol{y}; \boldsymbol{z})] \boldsymbol{\alpha} \cdot \boldsymbol{A}^b(\boldsymbol{z}), \tag{21}$$

where S, V, and W are variation kernels. Neglecting the coupling to the transversal gluons in the kernel ($V = W = 0$) leads to a variational equation for S alone, which corresponds to the well-known Adler-Davis model [25]. Next, we must shift the trial wave functionals to comply with the constraint $\langle A \rangle = \mathsf{a}$,

$$|\Phi_{\mathsf{a}}[A]\rangle = \mathcal{N} \mathcal{I}[A - \mathsf{a}]^{-\frac{1}{2}} \mathcal{J}_{\mathsf{a}}[A]^{-\frac{1}{2}} \tilde{\Phi}_{\text{YM}}[A - \mathsf{a}] |\Phi_q[A - \mathsf{a}]\rangle. \tag{22}$$

Notice that we have shifted the gauge field argument in all places *except* the Faddeev-Popov determinant $\mathcal{J}_{\mathsf{a}}[A]$, which was, however, changed from Coulomb gauge to background gauge, cf. Eq. (13). It is then easy to see that this wave functional indeed obeys the constraint $\langle A \rangle_{\Phi} = \mathsf{a}$;

in fact, the expectation value of *any* observable Ω in the state Eq. (22) is

$$\langle\Omega[\boldsymbol{A},\boldsymbol{\Pi},\psi]\rangle_{\mathsf{a}} = \langle\tilde{\Omega}[\boldsymbol{A}+\mathsf{a},\boldsymbol{\Pi},\psi]\rangle_0, \qquad (23)$$

with the modified observable $\tilde{\Omega}$

$$\tilde{\Omega}[\boldsymbol{A},\boldsymbol{\Pi},\psi] = \mathcal{J}_{\mathsf{a}}[\boldsymbol{A}]^{\frac{1}{2}}\mathcal{I}[\boldsymbol{A}-\mathsf{a}]^{\frac{1}{2}}\Omega[\boldsymbol{A},\boldsymbol{\Pi},\psi]\mathcal{J}_{\mathsf{a}}[\boldsymbol{A}]^{-\frac{1}{2}}\mathcal{I}[\boldsymbol{A}-\mathsf{a}]^{-\frac{1}{2}}, \tag{24}$$

which reduces to Ω if it contains no functional derivatives, i.e. if it does not depend on $\boldsymbol{\Pi}$. The expectation value $\langle\cdots\rangle_0$ on the rhs of Eq. (23) is with the same wave functionals Eqs. (19) and (21) as in Coulomb gauge (hence the subscript "0"), but with the fields $\boldsymbol{A}$ being background transversal $\hat{\mathsf{d}}\boldsymbol{A} = 0$, and with the kernel ω in Eq. (19) promoted to a matrix in adjoint color space. (This will be discussed in the next subsection.) If we take $\Omega[\boldsymbol{A}] = \boldsymbol{A}$, in particular, then we have $\tilde{\Omega}[\boldsymbol{A}+\mathsf{a}] = \boldsymbol{A}+\mathsf{a}$ and thus $\langle\boldsymbol{A}\rangle_{\mathsf{a}} = \langle\boldsymbol{A}+\mathsf{a}\rangle_0 = \mathsf{a}+\langle\boldsymbol{A}\rangle_0 = \mathsf{a}$, because $\langle\boldsymbol{A}\rangle_0 = 0$ in the original Coulomb gauge wave functional.

C. QCD propagators in the presence of a background field

To carry out the variational approach we have to compute the expectation value of the gauge-fixed QCD Hamiltonian in a trial wave functional (22),

$$\langle H_{\mathrm{fix}}\rangle_{\mathsf{a}} = \langle\tilde{H}_{\mathrm{fix}}[\boldsymbol{A}+\mathsf{a}]\rangle_0 = \langle H_{\mathrm{fix}}[\boldsymbol{A}+\mathsf{a}]\rangle_0 + \cdots, \qquad (25)$$

where the dots indicate higher order terms from moving the determinants in Eq. (24) past the momentum operators $\boldsymbol{\Pi}$ in H_{fix}. The gauge field is a connection and thus enters H_{fix} only through the covariant derivative; the same holds for the gauge condition $\hat{\mathsf{d}}_{\mathsf{a}}\boldsymbol{A} = 0$, while the trial wave functional used in $\langle\cdots\rangle_0$ are the ones from Coulomb gauge Eq. (18), which do not depend on the background field explicitly. As a consequence, the only effect of the background gauge field in $\langle H_{\mathrm{fix}}[\boldsymbol{A}+\mathsf{a}]\rangle_0$ as compared to Coulomb gauge $\mathsf{a} = 0$ is to replace all ordinary derivatives by covariant background derivatives, $\nabla \to \mathsf{d}_{\mathsf{a}} = \nabla + \mathsf{a}$. This, in turn, has the effect of shifting the momentum argument of Green's functions and the variation kernels.

To describe this shift, it is convenient to go to a color basis in which $\hat{\mathsf{d}}$ and $\hat{\mathsf{a}}$ are diagonal. First we expand the background field in the Cartan subalgebra,

$$\mathsf{a} = \sum_{k=1}^{r}\mathsf{a}_k H^k = \sum_{\mu}(-i\underline{\mathsf{a}}\cdot\underline{\mu})|\mu\rangle\langle\mu|, \qquad (26)$$

where r is the rank of the color group, H_k denotes the Cartan generators, and the weight vector $\underline{\mu} = (\mu_1,...,\mu_r)$ contains r eigenvalues of the H_k. [There are N distinct

weight vectors for $G = SU(N)$, each of which corresponds to one of the N distinct color vectors $|\mu\rangle$ which diagonalize the Cartan generators simultaneously.] A similar relation holds in the adjoint representation,

$$\hat{\mathsf{a}} = \sum_{\sigma}(-i\underline{\mathsf{a}}\cdot\underline{\sigma})|\sigma\rangle\langle\sigma|, \qquad (27)$$

where the (N^2-1) root vectors $\underline{\sigma} = (\sigma_1,...,\sigma_r)$ now contain eigenvalues of $\hat{H}_k$ in the adjoint, and the (N^2-1) eigenvectors $|\sigma\rangle$ are adjoint color vectors which diagonalize the $\hat{H}_k$ simultaneously. For further details, see Appendix A.

After expanding the fields and kernels in the trial wave functional in the Cartan basis we can Fourier transform them in the usual fashion based on translational invariance. The action of the covariant background derivative is then

$$\frac{1}{i}\mathsf{d}\exp(i\boldsymbol{px})) = \sum_{\mu}|\mu\rangle\langle\mu|\boldsymbol{p}^{\mu}\cdot\exp(i\boldsymbol{px}), \qquad \boldsymbol{p}^{\mu} = \boldsymbol{p} - \underline{\mathsf{a}}\cdot\underline{\mu}, \tag{28}$$

$$\frac{1}{i}\hat{\mathsf{d}}\exp(i\boldsymbol{px}) = \sum_{\sigma}|\sigma\rangle\langle\sigma|\boldsymbol{p}^{\sigma}\cdot\exp(i\boldsymbol{px}), \qquad \boldsymbol{p}^{\sigma} = \boldsymbol{p} - \underline{\mathsf{a}}\cdot\underline{\sigma}. \tag{29}$$

Since this is the only way in which the background field enters, we can conclude that the only modification introduced by a constant background field a in the Cartan algebra is (i) to expand all color fields in the weight or root vectors, as appropriate, and (ii) to shift a momentum variable by $(-\underline{\mathsf{a}}\cdot\underline{\mu})$ if it is associated with a quark field, and by $(-\underline{\mathsf{a}}\cdot\underline{\sigma})$ for gluons and ghosts.

D. The variational approach in the presence of the background field

We are now in a position to compute the expectation value of the full gauge fixed QCD Hamiltonian in our trial wave functional (22) depending explicitly on the background field a,

$$\langle H_{\mathrm{fix}}\rangle_{\mathsf{a}} = \langle H_{\mathrm{YM}}^{\perp}\rangle_{\mathsf{a}} + \langle H_q\rangle_{\mathsf{a}} + \langle H_C\rangle_{\mathsf{a}}. \qquad (30)$$

The first (Yang-Mills) piece can be further expanded into three contributions,

$$\langle H_{\mathrm{YM}}^{\perp}\rangle_{\mathsf{a}} = \langle H_{\mathrm{YM}}^{A}\rangle_{\mathsf{a}} + \langle H_{\mathrm{YM}}^{\mathrm{NA}}\rangle_{\mathsf{a}} + \langle H_{\mathrm{YM}}^{q}\rangle_{\mathsf{a}}. \qquad (31)$$

The first term contains the kinetic (electric) energy plus the Abelian part of the magnetic energy. It is a 1-loop contribution and involves only the variational kernel ω and the curvature χ (see below). The second term is the contribution from the non-Abelian part of the magnetic energy. In the gluon gap equation, it only contributes a

(divergent) constant and is hence often neglected. Below, we will show that the finite reminder of this constant after renormalization may, however, have a significant impact on the Polyakov loop; the non-Abelian magnetic energy will be discussed in more detail in Sec. V. The third term comes from the action of the canonical momentum operator $\mathbf{\Pi}$ on the A-dependent part of the quark wave function. It is a 2-loop term that vanishes if $V = W = 0$, since then the quark wave functional (20) does not couple to A.

In the quark sector, H_q contains no momentum operator $\mathbf{\Pi}$ and the prescription Eq. (23) yields two contributions

$$\langle H_q[A]\rangle_{\mathsf{a}} = \langle H_q[A+\mathsf{a}]\rangle_0 = \langle H_q^{\mathsf{a}}\rangle_0 + \langle H_q^A\rangle_0, \quad (32)$$

where

$$H_q^{\mathsf{a}} = -i \int d^3x\, \psi^\dagger(\mathbf{x})\boldsymbol{\alpha}\cdot\mathsf{d}(\mathbf{x})\psi(\mathbf{x}), \qquad (33)$$

$$H_q^A = -i \int d^3x\, \psi^\dagger(\mathbf{x})\boldsymbol{\alpha}\cdot A(\mathbf{x})\psi(\mathbf{x}). \qquad (34)$$

The second term Eq. (34) is again a 2-loop contribution that vanishes if $V = W = 0$, because then the expectation value factorizes and $\langle A\rangle_0 = 0$. The first term Eq. (33) has both a 1-loop contribution that only depends on the scalar quark kernel S (see below), and a 2-loop contribution that vanishes if $V = W = 0$.

Finally, the Coulomb term couples the charge densities $\rho_{\mathrm{tot}} = \rho + \rho_{\mathrm{YM}}$ of the gluon and quark. This gives three contributions according to the combination of the charges involved,

$$\langle H_C\rangle_{\mathsf{a}} = \underbrace{\langle H_C^A\rangle_{\mathsf{a}}}_{\sim\rho_{\mathrm{YM}}\cdot\rho_{\mathrm{YM}}} + \underbrace{\langle H_C^q\rangle_{\mathsf{a}}}_{\sim\rho\cdot\rho} + \underbrace{\langle H_C^{\mathrm{mix}}\rangle_{\mathsf{a}}}_{\sim\rho\cdot\rho_{\mathrm{YM}}}. \qquad (35)$$

All three contributions are 2-loop terms. The mixed contribution describes an interaction between gluons and quarks which is not expected to have a significant effect on the Polyakov loop (an interquark potential!) to this order. We will neglect the mixed contribution in the following. The quark part $\langle H_C^q\rangle_{\mathsf{a}}$ of the Coulomb interaction is included in the quark gap equation, cf. Sec. III B below, and the gluon part $\langle H_C^A\rangle_{\mathsf{a}}$ is studied in more detail in Sec. V.

Putting everything together, we can split the full QCD expectation value in our background gauge trial wave functional in a bosonic and a fermionic part,

$$\langle H_{\mathrm{fix}}\rangle_{\mathsf{a}} = E_B[\mathsf{a}] + E_F[\mathsf{a}]. \qquad (36)$$

Both terms have 1- and 2-loop contributions according to the following chart:

$$E_B[\mathsf{a}] = \underset{\substack{\downarrow\\ \text{1-loop}\,(\omega,\chi)}}{\langle H_{\mathrm{YM}}^A\rangle_{\mathsf{a}}} + \underset{\substack{\downarrow\\ \text{2-loop}\,(\omega,\chi)}}{\langle H_{\mathrm{YM}}^{\mathrm{NA}}\rangle_{\mathsf{a}}} + \underset{\substack{\downarrow\\ \text{2-loop}\,(\rho_{\mathrm{YM}}\rho_{\mathrm{YM}})}}{\langle H_C^A\rangle_{\mathsf{a}}} + \underset{\substack{\downarrow\\ \text{2-loop}\,(V,W)}}{\langle H_{\mathrm{YM}}^q\rangle_{\mathsf{a}}},$$
$$(37)$$

$$E_F[\mathsf{a}] = \underset{\substack{\downarrow\\ \text{1-loop}\,(S)\\ \text{2-loop}\,(V,W,S)}}{\langle H_q^{\mathsf{a}}\rangle_0} + \underset{\substack{\downarrow\\ \text{2-loop}\,(V,W)}}{\langle H_q^A\rangle_0} + \underset{\substack{\downarrow\\ \text{2-loop}\,(V,W)}}{\langle H_C^q\rangle_{\mathsf{a}}} + \underset{\substack{\downarrow\\ \text{2-loop}\,(\rho_{\mathrm{YM}}\rho)}}{\langle H_C^{\mathrm{mix}}\rangle_{\mathsf{a}}}.$$
$$(38)$$

The arrows indicate the variation kernels ω, S, V, W on which the respective contribution depends. If we set $V = W = 0$ and hence employ a BCS type of wave functional for the quarks, and further neglect the mixed 2-loop Coulomb interactions involving both ρ and ρ_{YM}, then the result simplifies considerably:

$$E_B[\mathsf{a}] = \langle H_{\mathrm{YM}}^A\rangle_{\mathsf{a}} + \langle H_{\mathrm{YM}}^{\mathrm{NA}}\rangle_{\mathsf{a}} + \langle H_C^A\rangle_{\mathsf{a}}, \qquad (39)$$

$$E_F[\mathsf{a}] = \langle H_q^{\mathsf{a}}\rangle_0 + \langle H_C^q\rangle_{\mathsf{a}}. \qquad (40)$$

The first term in both the fermionic and bosonic contributions is 1-loop, while the remaining terms are all 2-loop contributions.

E. Hamiltonian dynamics at finite temperature

The developments made so far allow for a computation of the minimal energy $\langle H_{\mathrm{fix}}\rangle_\Phi$ in all states obeying the background field constraint $\langle A\rangle_\Phi = \mathsf{a}$, or at least for a subset of states characterized by our *Ansatz* (18). This minimal energy is the effective potential of the Polyakov loop background a at $T = 0$.

As we switch on the temperature, the variational principle still determines the minimal energy, when we are actually interested in the *free* energy. The reason for this shortcoming is that our trial *Ansatz* Eq. (18) is no longer sufficient at finite temperature: we should instead work with thermal states that involve arbitrary excitations above the ground state within a grand canonical ensemble. Such an approach has been attempted [19], but there is a simpler formulation which allows us to work with a trial vacuum wave functional and the usual minimization of the ground state energy [21,22,26]. The finite temperature $T = \beta^{-1}$ is here introduced by a compactification of the x_3 direction via the boundary conditions

$$\psi^m(x_1, x_2, x_3 = \beta/2) = -\psi^m(x_1, x_2, x_3 = -\beta/2), \quad (41\mathrm{a})$$

$$A^a(x_1, x_2, x_3 = \beta/2) = A^a(x_1, x_2, x_3 = -\beta/2) \quad (41\mathrm{b})$$

for the quark and gluon field, respectively. With these conditions, the original space manifold is effectively

compactified to a cylinder $\mathbb{R}^2 \times S^1(\beta)$, and we use the abbreviation

$$\int_\beta d^3x \equiv \lim_{\ell \to \infty} \int_{-\ell/2}^{\ell/2} dx_1 \int_{-\ell/2}^{\ell/2} dx_2 \int_{-\beta/2}^{\beta/2} dx_3 \quad (42)$$

for the spatial integration over this manifold. The length ℓ of the uncompactified direction will always be large, and the limit $\ell \to \infty$ projects out the grand canonical partition function of QCD at nonzero temperature T and chemical potential μ [20]

$$\mathcal{Z} = \lim_{\ell \to \infty} \exp[-\ell E_0(\beta, \mu)], \quad (43)$$

where E_0 is the smallest eigenvalue of the non-Hermitian pseudo-Hamiltonian

$$\tilde{H}(\beta, \mu) \equiv \int_\beta \mathcal{H} + i\mu \int_\beta d^3x \, \psi^\dagger(x) \alpha_3 \psi(x). \quad (44)$$

Here, $\mathcal{H}$ is the usual QCD Hamiltonian density in Coulomb and Weyl gauge [27], and α_3 one of the Dirac matrices.

It should be emphasized that the analysis of Ref. [20] exchanges the Euclidean time direction x_0 with x_3 (and likewise for all vector quantities) assuming relativistic $O(4)$ invariance of the underlying Euclidean field theory. In particular, it does not hold for nonrelativistic quark models or effective nuclear theories that single out a fixed reference frame. For the case of a vanishing chemical potential $\mu = 0$, the Hamiltonian $\tilde{H}(\beta, 0)$ is Hermitian, all energy eigenvalues are real and the limit $\ell \to \infty$ of the noncompactified directions projects out the ground state contribution in Eq. (43). (For $\mu \neq 0$ and real, the situation is more complicated and we defer $\mu \neq 0$ to a forthcoming investigation.)

For explicit calculations, it is convenient to switch to momentum space. From the general boundary conditions Eq. (41a), continuity of the wave functional implies, for instance, for the quark kernel,

$$K(x + \beta e_3, y) = K(x, y + \beta e_3) = -K(x, y), \quad (45)$$

and a similar relation for the scalar dressing function $S(x - y)$ if we set $V = W = 0$. The Fourier representation thus takes the form

$$S(x) = \int_\beta d^3p \, \exp[i(p_\perp + \tilde{\Omega}_n e_3) \cdot x] S(p_\perp, \tilde{\Omega}_n), \quad (46)$$

where $p_\perp = p_1 e_1 + p_2 e_2$ is the planar momentum perpendicular to the compactified direction of the heat bath, and

$$\tilde{\Omega}_n = \frac{\pi(2n + 1)}{\beta}, \qquad n \in \mathbb{Z} \quad (47)$$

are the fermionic Matsubara frequencies. Furthermore, we have introduced the short-hand notation

$$\int_\beta d^3p \cdots \equiv \int \frac{d^2p_\perp}{(2\pi)^2} \frac{1}{\beta} \sum_{n=-\infty}^\infty \cdots. \quad (48)$$

A similar relation holds for the bosonic kernel ω, with the bosonic Matsubara frequencies

$$\Omega_n = \frac{2\pi n}{\beta}, \qquad n \in \mathbb{Z}. \quad (49)$$

III. THE EFFECTIVE POTENTIAL OF THE POLYAKOV LOOP AT 1-LOOP

We are now in the position to compute the effective potential of the background field representing the Polyakov loop. We start with the 1-loop contributions in Eqs. (39) and (40). Since the background field a in 3-direction is constant, the space volume always factorizes and we really compute the energy *density* $e[a] = E_B[a]/V_3 = E_B[a]/(V_\perp \beta)$.

A. Boson contribution

We begin with the bosonic 1-loop contribution in Eq. (39). A straightforward calculation at $T = 0$ gives [22]

$$e_B[a] = \sum_\sigma \int \frac{d^3p}{(2\pi)^3} [\omega_\sigma(p) - \chi_\sigma(p)], \quad (50)$$

where the sum is over all roots σ of $SU(N)$. The curvature $\chi(k)$ is the contribution from the ghost loop which can be related to the ghost form factor and the gluon kernel ω through a separate DSE [23]. As explained before, the background field a lives in the Cartan subalgebra and is taken to be constant in the 3-direction. It enters $\langle H_{YM}^A \rangle_a$ only through the covariant derivative when using Eq. (23), and the kernels $\omega_\sigma(p)$ and $\chi_\sigma(p)$ are hence obtained from their $T = 0$ counterparts through a shift $p \to p^\sigma$ in the momentum argument, $\omega_\sigma(p) = \omega(p^\sigma)$, cf. Eq. (29). This prescription can also be seen explicitly in the DSE for the curvature χ_σ and the gap equation obtained by minimizing the bosonic energy,

$$\omega_\sigma(p)^2 = p_\sigma^2 + \chi_\sigma(p)^2 + I_0^{NA} + I_C^A(p, \sigma). \quad (51)$$

Here, I_0^{NA} is a (colorless) tadpole term from the non-Abelian part of the magnetic energy in Eq. (39), while I_C^A comes from the 2-loop Coulomb term in Eq. (39). Both expressions are divergent and require renormalization, cf. Sec. III C below. Let us mention at this point already that the renormalization of the tadpole term I_0^{NA} requires a gluon mass counterterm, cf. Eq. (82) below. If the coefficient is adjusted to cancel the divergences in I_0^{NA} at zero

temperature, then we expect no further divergences to appear (from this term) at finite temperature and non-vanishing background field. This is indeed the case, though the explicit verification is rather tricky, cf. Sec. V A. For the logarithmic divergence in the Coulomb 2-loop term I_C^A, we do not as yet have a full renormalization at finite temperature. In the present paper, we will take a more pragmatic approach and identify, isolate and then subtract the divergence as usual. The remaining free parts are not fixed by a renormalization condition at $T = 0$, but we treat the corresponding counterterm coefficient as a free parameter.

It should be emphasized that Eq. (50) is the *self-consistent* energy obtained after inserting the gap equation into the full energy and truncating at 1-loop level. Since the gap equation mixes loop orders, it will thus effectively contain 2-loop contributions. We must hence ensure that Eq. (51) holds—maybe in renormalized form—when using Eq. (50). The quark sector does not couple directly to the gluon sector at this level, provided that we also waive the direct coupling of the quarks to the gluon field A in the trial wave function, i.e. we set the kernels $V = W = 0$. In this case, the gluon sector is identical to the Yang-Mills case, and we refer to Ref. [23] for a detailed discussion of the boson kernels ω and χ at $T = 0$. The 2-loop terms missing in Eq. (50) will be discussed in Sec. V below.

As we switch on the temperature, the initial $O(3)$ rotation symmetry is broken, and the kernel ω can no longer be transversal. Instead, the compactification of the 3-direction gives rise to two distinct Lorentz structures, $\omega = \omega^\perp t^\perp + \omega^\parallel r t^\parallel$, where the projectors are (at $\mathsf{a} = 0$ for simplicity [23])

$$t_{ij}^\perp(\boldsymbol{p}) = (1 - \delta_{i3})\left(\delta_{ij} - \frac{p_i p_j}{\boldsymbol{p}_\perp^2}\right)(1 - \delta_{j3}),$$
$$t_{ij}^\parallel(\boldsymbol{p}) = t_{ij}(\boldsymbol{p}) - t_{ij}^\perp(\boldsymbol{p}). \qquad (52)$$

As indicated, the two distinct Lorentz structures involve two distinct scalar variation kernels $\omega^\perp(\boldsymbol{p})$ and $\omega^\parallel(\boldsymbol{p})$, and likewise for the curvature χ. The Lorentz trace of the boson kernel, previously $\mathrm{tr}\omega = 2\omega(\boldsymbol{p})$, now becomes

$$\mathrm{tr}\omega = \omega^\perp(\boldsymbol{p})\mathrm{tr}t^\perp(\boldsymbol{p}) + \omega^\parallel(\boldsymbol{p})\mathrm{tr}t^\parallel(\boldsymbol{p}) = \omega^\perp(\boldsymbol{p}) + \omega^\parallel(\boldsymbol{p}),$$

and the color trace turns into the sum over roots. Finally, the integration in the compactified dimension is replaced by a Matsubara sum and Eq. (50) turns into

$$e_B(\mathsf{a}, \beta) = \frac{1}{2}\sum_\sigma \int \frac{d^2 p_\perp}{(2\pi)^2}\frac{1}{\beta}\sum_{n\in\mathbb{Z}}[\omega^\perp(\boldsymbol{p}_n^\sigma) - \chi^\perp(\boldsymbol{p}_n^\sigma)$$
$$+ \omega^\parallel(\boldsymbol{p}_n^\sigma) - \chi^\parallel(\boldsymbol{p}_n^\sigma)], \qquad (53)$$

where we have now applied the shift as in Eq. (29),

$$\boldsymbol{p} \mapsto \boldsymbol{p}_n^\sigma \equiv \boldsymbol{p}_\perp + (\Omega_n - \underline{\sigma}\cdot\underline{\mathsf{a}})\hat{\boldsymbol{e}}_3, \qquad \Omega_n \equiv 2\pi n/\beta. \quad (54)$$

The quantity Eq. (53) is still infinite because it contains the (free) energy of the vacuum. Since the Polyakov loop represents a single static quark immersed in the thermal QCD ground state, its effective potential must be understood as the *change* of the free energy due to the presence of the background,

$$\bar{e}(\mathsf{a}, \beta) \equiv e(\mathsf{a}, \beta) - e(0, \beta). \qquad (55)$$

The subtraction is most easily performed after Poisson resumming the Matsubara sum,[2]

$$\bar{e}_B(\mathsf{a}, \beta) = \sum_\sigma \int \mathrm{d}^3 p \sum_{m\in\mathbb{Z}} e^{im\beta p_z}[g_B(\boldsymbol{p}^\sigma) - g_B(\boldsymbol{p})], \qquad (57)$$

where $\boldsymbol{p}^\sigma = \boldsymbol{p}_\perp + \boldsymbol{e}_3(p_z - \mathsf{a}\cdot\underline{\sigma})$, and we have defined

$$g_B(\boldsymbol{p}) \equiv \frac{1}{2}[\omega^\perp(\boldsymbol{p}) - \chi^\perp(\boldsymbol{p}) + \omega^\parallel(\boldsymbol{p}) - \chi^\parallel(\boldsymbol{p})]. \quad (58)$$

Next we shift $p_z \to p_z + \mathsf{a}\cdot\underline{\sigma}$ and introduce the dimensionless background shift

$$\Delta^\sigma \equiv \frac{\beta}{2\pi}(\mathsf{a}\cdot\underline{\sigma}). \qquad (59)$$

This gives

$$\bar{e}_B(\mathsf{a}, \beta) = \sum_\sigma \sum_{m\in\mathbb{Z}} \int \mathrm{d}^3 p \, e^{im\beta p_z}[e^{2\pi im\Delta^\sigma} - 1]g_B(\boldsymbol{p}). \quad (60)$$

Due to the subtraction Eq. (55), the term with $m = 0$, i.e. the vacuum energy at $T = 0$, does not contribute to this expression. Furthermore, the term in the bracket vanishes for the trivial root $\sigma = (0, 0, \dots)$, while the nontrivial roots of $SU(N)$ always come in pairs with an opposite sign, so that

$$\sum_\sigma [e^{2\pi im\Delta^\sigma} - 1] = -\sum_\sigma [1 - \cos(2\pi m\Delta^\sigma)].$$

Equation (60) can now be rewritten as

---

[2]This technique is based on the simple distributional identity

$$\frac{1}{\beta}\sum_{n=-\infty}^\infty u(\Omega_n) = \frac{1}{\beta}\sum_{n=-\infty}^\infty u\left(\frac{2\pi n + \varphi}{\beta}\right)$$
$$= \int_{-\infty}^\infty \frac{dp_3}{2\pi}\sum_{m=-\infty}^\infty \exp[im(\beta q_3 - \varphi)]u(q_3), \quad (56)$$

which is valid for suitable test functions u and arbitrary $\varphi \in [0, 2\pi]$. The case $\varphi = 0$ corresponds to bosons, $\varphi = \pi$ to fermions.

$$\bar{e}_B(\mathsf{a},\beta) = -2\sum_\sigma \sum_{\mathsf{m}=1}^\infty [1 - \cos(2\pi\mathsf{m}\Delta^\sigma)]$$

$$\times \int \mathrm{d}^3 p \, \cos(\mathsf{m}\beta p_z) g_B(\boldsymbol{p}). \qquad (61)$$

In the last step, we nondimensionalize the (free) energy density and rewrite it in a form suitable for later numerical evaluation:

$$u_B(\mathsf{a},\beta) \equiv \beta^4 [e_B(\mathsf{a},\beta) - e_B(0,\beta)]$$

$$= \frac{2}{\pi^2} \sum_{\mathsf{m}=1}^\infty \sum_\sigma \frac{1 - \cos(2\pi\mathsf{m}\Delta^\sigma)}{\mathsf{m}^4} h_B(\beta\mathsf{m}), \quad (62)$$

$$h_B(\lambda) = -\pi^2 \lambda^4 \mathsf{Re} \int \mathrm{d}^3 p \, e^{i\lambda p_z} g_B(\boldsymbol{p}). \qquad (63)$$

The temperature dependence is completely encoded in the function $h_B(\lambda)$. We compute it by introducing spherical coordinates (p, ϑ, φ) for $\boldsymbol{p}$ and note that the polar angle φ is cyclic due to the residual $O(2)$ symmetry in the xy plane mentioned above. Changing variables $\vartheta \to \xi \equiv \cos\vartheta$, we obtain

$$h_B(\lambda) = -\frac{\lambda^4}{4} \int_0^\infty dp \, p^2 \int_{-1}^1 d\xi \, \cos(\lambda p\xi) g_B(p,\xi). \qquad (64)$$

Since $\omega(\boldsymbol{p}) \sim p$ and $\chi(\boldsymbol{p}) \sim 1/p$ at large p, we also have $g_B(\boldsymbol{p}) \sim p$ for $p \to \infty$ and Eq. (64) is apparently UV divergent. We will investigate this issue in more detail in Sec. III C. If the kernels happen to be $O(3)$ symmetric, i.e. if they do not depend on the angle against the heat bath, the ξ integration can be performed and we obtain

$$h_B(\lambda) = -\frac{\lambda^3}{2} \int_0^\infty dp \, p \, \sin(\lambda p) g_B(p). \qquad (65)$$

Even if we do not have $O(3)$ symmetry, we can still use Eq. (65) with the $g_B(p)$ replaced by the angular average

$$\bar{g}_B(p) \equiv \frac{\lambda}{2} \int_{-1}^{+1} d\xi \frac{\cos(\lambda p\xi)}{\sin(\lambda p)} p g_B(p,\xi)$$

$$\to \frac{1}{2} \int_{-1}^1 d\xi \, g_B(p,\xi) \quad \text{at } \lambda \to 0. \qquad (66)$$

As indicated, this reduces to the simple integral average when $\lambda \ll 1$, i.e. at very high temperatures. Thus, for any finite temperature kernel, we can do the angular average Eq. (66) and then employ the $O(3)$ symmetric relations such as Eq. (65).

For $G = SU(2)$, the roots are $\{-1, 0, +1\}$, so that $\Delta^\sigma = \{-x, 0, +x\}$ in terms of the fundamental domain (*Weyl alcove*)

$$x \equiv \frac{\beta\mathsf{a}^3}{2\pi} \in [0,1], \qquad (67)$$

on which center symmetry acts by $x \to 1 - x$. The center symmetric point for $G = SU(2)$ is therefore $x = \frac{1}{2}$, while $x \in \{0, 1\}$ are the maximally center breaking points. The contribution of the trivial root drops out of the Poisson sum in Eq. (62) and we find

$$u_B(x,\beta) = \frac{4}{\pi^2} \sum_{\mathsf{m}=1}^\infty \frac{1 - \cos(2\pi\mathsf{m}x)}{\mathsf{m}^4} h_B(\mathsf{m}\beta), \qquad x \in [0,1]. \qquad (68)$$

To check this formula, recall that the 1-loop effective potential in *perturbation theory* requires only tree-level kernels, i.e. we can set $\omega_\perp(p) = \omega_\parallel(p) = p$ and $\chi_\perp(p) = \chi_\parallel(p) = 0$ to this order, so that $g_B(p) = p$ and hence, from Eq. (65), $h_B(\lambda) = 1$. (We will discuss the calculation of h_B and the treatment of the UV divergences below.) The corresponding effective potential for the Polyakov loop in $G = SU(2)$ is

$$u_B(x,\beta) = \frac{4}{\pi^2} \sum_{\mathsf{m}=1}^\infty \frac{1 - \cos(2\pi\mathsf{m}x)}{\mathsf{m}^4} = \frac{4}{3}\pi^2 x^2 (1 - |x|)^2,$$

$$x \in [-1,1]. \qquad (69)$$

This is indeed the Weiss potential [28] usually obtained in 1-loop thermal perturbation theory.

Let us also generalize Eq. (68) to the color group $SU(3)$ which has rank 2 so that the Polyakov loop background field has two color components, a^3 and a^8. As a parametrization of the Polyakov loop (or the Weyl alcove), we choose

$$x \equiv \frac{\beta\mathsf{a}^3}{2\pi} \in [0,1],$$

$$y \equiv \frac{\beta\mathsf{a}^8}{2\pi} \in [0, 2/\sqrt{3}]. \qquad (70)$$

Since the Weyl alcove for $G = SU(3)$ is triangular, the square region for (x, y) defined above actually covers a single Weyl alcove plus two adjacent half-alcoves. The effective potential of the $SU(3)$ Polyakov loop background is again given by Eq. (57); the only difference to $G = SU(2)$ is the root sum, which now runs over $N^2 - 1 = 8$ root vectors, of which $N(N-1) = 6$ are nonvanishing. The nonzero roots come in pairs with both signs, and the three nonvanishing *positive* roots lead to different momentum shifts. After performing the root sum, it follows that the
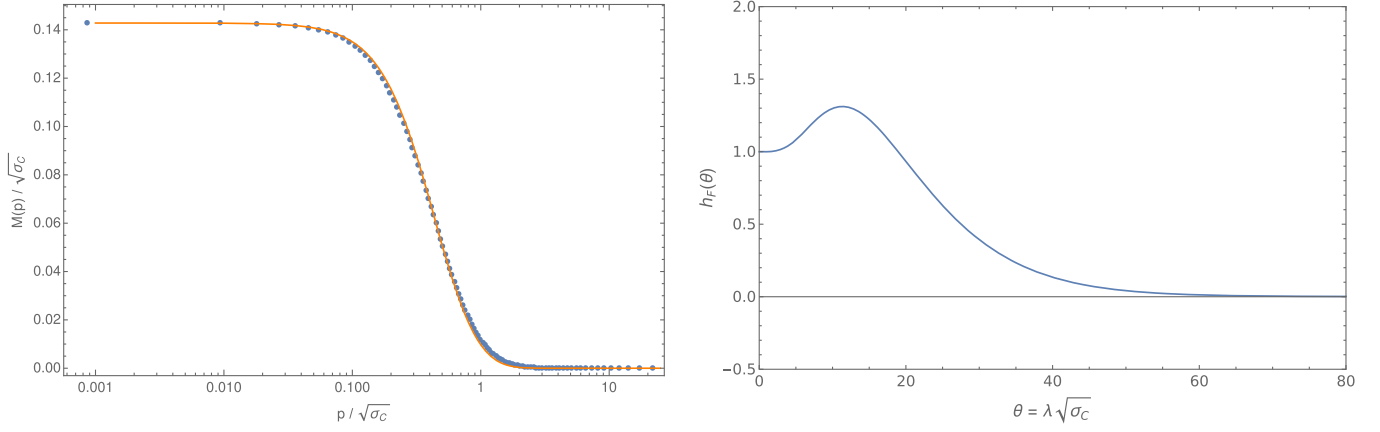
FIG. 1.   Left: smooth fit to the numerical solution of the Adler-Davis equation. Right: the Fourier transform $h_F(\lambda)$ for fermions; the dimensionfull argument λ is measured in units of $\sqrt{\sigma_c}$.

bosonic $SU(3)$ Polyakov loop potential is simply a sum of three $SU(2)$ potentials,

$$u_B(x, y, \beta) = u_B(x, \beta) + u_B\left(\frac{x + y\sqrt{3}}{2}, \beta\right)$$

$$+ u_B\left(\frac{x - y\sqrt{3}}{2}, \beta\right). \tag{71}$$

B. Fermion 1-loop contribution

In the present study, we waive the explicit coupling to the gluon sector in the trial wave functional ($V = W = 0$), so that only a single scalar variation kernel $S(\boldsymbol{p})$ remains in the quark sector. The corresponding expectation value to the Fermi part of the energy in Eq. (40) contains a 1-loop term involving the free quark Hamiltonian, and a 2-loop contribution involving the Coulomb potential. We proceed as in the boson case and first vary the total fermion energy with respect to the kernel $S(\boldsymbol{p})$ to obtain a fermionic gap equation. The solution, which relates 1- and 2-loop orders, is then inserted back into Eq. (40) to obtain the *self-consistent* quark energy up to and including 2-loop order. At this stage (and not earlier), the fermion energy is truncated to 1-loop order; through the gap equation, it will actually contain parts of the 2-loop term in Eq. (40), in a self-consistent manner.[3]

In more detail, the fermion gap equation is best formulated in terms of the *mass function $M(\boldsymbol{p})$*, which follows from the variational kernel $S(\boldsymbol{p})$ via

$$M(\boldsymbol{p}) = 2|\boldsymbol{p}| \cdot \frac{S(\boldsymbol{p})}{1 - S^2(\boldsymbol{p})}. \tag{72}$$

The value $M(0)$ can be viewed as a dynamically generated quark mass which breaks chiral symmetry. In the case of a vanishing background field $\mathsf{a} = 0$, the fermion gap equation formally agrees with the model proposed by Adler and Davis [25]

$$M(k) = m + \frac{C_F}{8\pi^2} \int_0^\infty dq \int_{-1}^1 dz \, q^2 V_C(q)$$

$$\times \frac{M(Q) - [1 + qz/k]M(k)}{\sqrt{Q^2 + M(Q)^2}}. \tag{73}$$

Here, $Q = |\boldsymbol{k} + \boldsymbol{q}| = \sqrt{k^2 + q^2 + 2kqz}$ and $C_F = \frac{N^2 - 1}{2N}$ is the value of the quadratic Casimir of the color group $SU(N)$. Initially, the gap equation also involves the non-Abelian Coulomb kernel, Eq. (16), which can however be replaced, to this order, by its vacuum expectation value $g^2\langle \hat{F}^{ab}(\boldsymbol{x}, \boldsymbol{y})\rangle \approx \delta^{ab} V_C(\boldsymbol{x}, \boldsymbol{y})$. The long-ranged part of the variational solution in the Yang-Mills sector is well described by a linear rising Coulomb potential, $V_C = -\sigma_C|\boldsymbol{x} - \boldsymbol{y}|$, which amounts to the Fourier transform $V_C(p) = 8\pi\sigma_C/p^4$ to be used in Eq. (73). The numerical solution for the mass function $M(p)$ at $T = 0$ is shown in the left panel of Fig. 1.

Next we insert the solution of Eq. (73) back into Eq. (40) and introduce finite temperature as before. After a straightforward calculation, we can employ the Poisson resummation formula (56) for fermions to obtain

$$e_F(\mathsf{a}, \beta) = -N_f \sum_\mu \int \mathrm{d}^3 p \sum_{\mathfrak{m}=-\infty}^\infty e^{i\beta\mathfrak{m}(p_z - \pi/\beta)}$$

$$\times \frac{p_\perp^2 + (p_z^\mu)^2}{\sqrt{p_\perp^2 + (p_z^\mu)^2 + M(\boldsymbol{p}^\mu)}}. \tag{74}$$

Here, N_f is the number of (light) quark flavors, the z component in the momentum variable $\boldsymbol{p}^\mu$ is shifted according to $p_z^\mu = p_z - \mathsf{a} \cdot \underline{\mu}$, and the sum is over all weights μ of

---

[3]If we truncated the energy to 1-loop order *prior* to the variation, the gap equation (73) would turn into $M(k) = m$, i.e. the Coulomb interaction and chiral symmetry breaking would be absent.

$SU(N)$. The remaining calculation also follows the bosonic case: we shift the integration variable $p_z \to p_z + \mathsf{a} \cdot \mu$, Poisson resum the Matsubara series and subtract the vacuum contribution ($\mathsf{a} = 0$). For the result, we introduce the quantities

$$\Delta^\mu = \frac{\beta}{2\pi}(\mathsf{a} \cdot \underline{\mu}), \qquad g_F(\boldsymbol{p}) = \frac{\boldsymbol{p}^2}{\sqrt{\boldsymbol{p}^2 + M(\boldsymbol{p})^2}}, \quad (75)$$

and the self-consistent quark contribution to the effective potential of the Polyakov loop becomes, at 1-loop level,

$$u_F(\mathsf{a}, \beta) \equiv \beta^4[e_F(\mathsf{a}, \beta) - e_F(0, \beta)]$$
$$= -\frac{N_f}{\pi^2} \sum_{\mathfrak{m}=-\infty}^{\infty} (-1)^{\mathfrak{m}} \frac{\sum_\mu [1 - e^{2\pi i \mathfrak{m} \Delta^\mu}]}{\mathfrak{m}^4} h_F(\beta\mathfrak{m}), \quad (76)$$

$$h_F(\lambda) = -\pi^2 \lambda^4 \mathsf{Re} \int \mathfrak{d}^3 p \, e^{i\lambda p_z} g_F(\boldsymbol{p})$$
$$= -\frac{\lambda^3}{2} \int_0^\infty dp \, p \sin(\lambda p) g_F(p). \quad (77)$$

As indicated, only the real part of the Fourier integral contributes, because $g_F(\boldsymbol{p})$ must be even under the flip[4] $p_z \to (-p_z)$. Upon comparing Eq. (63) with Eq. (77), we realize that the factors $h_B(\lambda)$ and $h_F(\lambda)$ are constructed in the same way, with $g_B(\boldsymbol{p})$ in the bosonic case replaced by $g_F(\boldsymbol{p})$ in the fermionic case.

Next we compute the weight sum in Eq. (76). For $G = SU(2)$, the fundamental representation is two dimensional and we have hence two weights $\mu = \pm 1/2$ so that $\Delta^\mu = (\mathsf{a} \cdot \underline{\mu})\beta/(2\pi) = \pm\beta\mathsf{a}/(4\pi) = \pm x/2$. After a short calculation,

$$u_F(x, \beta) = -\frac{4N_f}{\pi^2} \sum_{\mathfrak{m}=1}^{\infty} (-1)^{\mathfrak{m}} \frac{1 - \cos(\pi\mathfrak{m}x)}{\mathfrak{m}^4} h_F(\beta\mathfrak{m}). \quad (78)$$

For $G = SU(3)$, the fundamental representation is three dimensional and we have thus three weights

$$\underline{\mu}_1 = \frac{1}{2}\begin{pmatrix} 1 \\ 1/\sqrt{3} \end{pmatrix}, \quad \underline{\mu}_2 = \frac{1}{2}\begin{pmatrix} -1 \\ 1/\sqrt{3} \end{pmatrix}, \quad \underline{\mu}_3 = \begin{pmatrix} 0 \\ -1/\sqrt{3} \end{pmatrix},$$

so that $\Delta^{1,2} = (\pm x + y/\sqrt{3})/2$ and $\Delta^3 = -y/\sqrt{3}$. The weight sum now becomes

---

$$\sum_\mu [1 - e^{2\pi i \mathfrak{m} \Delta^\mu}] = \sum_\theta [1 - \cos(\pi\mathfrak{m}\theta)] + \text{terms odd in } \mathfrak{m}, \quad (79)$$

where θ runs over the three values $\pm x + y/\sqrt{3}$ and $-2y/\sqrt{3}$. The terms odd in $\mathfrak{m}$ drop out in Eq. (76), because $h_F(-\lambda) = h_F(\lambda)$ as explained earlier. Furthermore, the term with $\mathfrak{m} = 0$ does not contribute due to the subtraction of the trivial background. Combining terms with $(\pm\mathfrak{m})$, we can again express the $SU(3)$ result as a sum over $SU(2)$ potentials,

$$u_F(x, y, \beta) = \frac{1}{2}\left[u_F\left(x + \frac{y}{\sqrt{3}}, \beta\right) + u_F\left(-x + \frac{y}{\sqrt{3}}, \beta\right) \right.$$
$$\left. + u_F\left(-2\frac{y}{\sqrt{3}}, \beta\right) \right]. \quad (80)$$

To check these equations, consider a free massless fermion, $M(p) = 0$, where $g_F(p) = p$ and hence $h_F(\lambda) = 1$ as in the bosonic case. The *perturbative* quark contribution to the effective potential of the $SU(2)$ Polyakov loop is therefore

$$u_F(x, \beta) = -\frac{4N_f}{\pi^2} \sum_{\mathfrak{m}=1}^{\infty} (-1)^{\mathfrak{m}} \frac{1 - \cos(\pi\mathfrak{m}x)}{\mathfrak{m}^4}$$
$$= N_f \frac{\pi^2}{6}\left(x^2 - \frac{1}{2}x^4 \right), \qquad x \in [-1, 1]. \quad (81)$$

This 1-loop result agrees with the quark part of the standard expression [28].

C. Renormalization and 1-loop numerics

Let us next study the counterterms necessary to render the bosonic gap equation (51) finite. [At $V = W = 0$, the fermionic gap equation (73) is UV finite if only the long-ranged part of the Coulomb potential is retained.] The quadratically divergent tadpole contribution I_0^{NA} is canceled by a gluon mass counterterm of the form [29]

$$H_{ct} = \frac{C_0}{2g^2} \int d^x A^a(\boldsymbol{x}) A^a(\boldsymbol{x}). \quad (82)$$

When added to the original Hamiltonian, this contributes the constant C_0 to the gap equation, which then takes the form

$$\omega_\sigma(\boldsymbol{p})^2 = p_\sigma^2 + \chi_\sigma(\boldsymbol{p})^2 + I_0^{NA} + C_0 + I_C^A(\boldsymbol{p}, \sigma). \quad (83)$$

The Coulomb term is a 2-loop contribution which also requires renormalization and an additional counterterm [29]. This is discussed in detail in Sec. V. For the moment,

it is sufficient to note that the relevant counterterm (with coefficient C_1) would result in the modified gap equation

$$\omega_\sigma(\boldsymbol{p})^2 = p_\sigma^2 + \chi_\sigma(\boldsymbol{p})^2 + [I_0^{NA} + C_0] + [I_C^A(k,\sigma) + 2C_1\chi(\boldsymbol{p})].$$
(84)

Numerical investigations [9] show that the last term in Eq. (84) can safely be neglected in the gap equation—it may, however, contribute in the total energy and this is investigated in Sec. V below. The remaining terms yield a gluon and ghost propagator that agrees very well with the lattice calculations [30] and, in particular, the analytical Gribov prediction. Furthermore, a perimeter law for the 't Hooft loop is only possible if the finite remainder of the last term in Eq. (84) vanishes [31]. All these arguments strongly suggest that the Coulomb term can be neglected in the gap equation, while it may play a significant role in the total energy.

The tadpole term I_0^{NA} depends on both the temperature and the background field but not the external momentum. We can therefore adjust the counterterm coefficient C_0 to cancel the quadratic divergence in the tadpole. The finite remainder,

$$c_0 \equiv I_0^{NA} + C_0,$$
(85)

is a free renormalization constant that should be fixed by either (i) relating it to another physical observable computed in the present scheme or (ii) fit the results for the Polyakov loop to lattice findings. Both methods cannot be fully carried out in the present formulation, since we have no suitable physical observable at our disposal, and the Polyakov loop in the confined phase of our formulation is qualitatively different from lattice findings, so that a fit is not meaningful. Instead, we treat c_0 as a *free* parameter and vary it to show what kind of results are possible with reasonable values of c_0. In this sense, our renormalization procedure requires future refinement to really pin down the physical value of c_0.

It is also important to note that the renormalization occurs without a background field and at zero temperature. It is generally expected that the divergences (and hence the counterterms) should be independent of temperature and the background field. This means that the sum of the temperature-dependent contributions from I_0^{NA} and the $T = 0$ counterterm must be UV finite. This is indeed the case, though the explicit proof is rather involved, cf. Sec. V.

Neglecting the Coulomb term as discussed above, the renormalized gap equation now takes the form (at $\mathsf{a} = 0$ and $T = 0$ for simplicity)

$$\omega(\boldsymbol{p})^2 = p^2 + \chi(\boldsymbol{p})^2 + c_0.$$
(86)

At the 1-loop level, we require no further counterterm. The DSE for the curvature may require a ghost wave function renormalization, but this is automatically included when we compute the curvature [at given $\omega(p)$] from the gap equation, rather than through its DSE. Before inserting the gap equation, the 1-loop boson energy density Eq. (53) including the counterterm becomes

$$e_B(\mathsf{a},\beta) = \sum_\sigma \int \mathrm{d}^3 p \, \frac{[\omega(p_\sigma) - \chi(p_\sigma)]^2 + \boldsymbol{p}_\sigma^2 + c_0}{\omega(p_\sigma)}, \quad (87)$$

where we have not distinguished the two Lorentz structures for simplicity. [We will only use the $T = 0$ solutions for $\omega(p)$ in the following.] Inserting the renormalized gap equation, the counterterm contribution formally drops out and we are left with

$$e_B(\mathsf{a},\beta) = \sum_\sigma \int \mathrm{d}^3 p [\omega(p_\sigma) - \chi(p_\sigma)],$$
(88)

just as in the unrenormalized case Eq. (53). The counterterm c_0 thus enters only indirectly via the modification of the curvature through the gap equation (86).

Even after renormalizing the gap equation, the profiles $h_B(\lambda)$ and $h_F(\lambda)$ entering the effective potential of the Polyakov loop are apparently UV divergent. Since these divergences cannot be canceled by any $T = 0$ counterterm in the theory, they must be spurious. To see this, note that the $T = 0$ vacuum energy (including all possible divergences and counterterms) is already subtracted in Eqs. (62) and (76), respectively, so that h_B and h_F may not contain ($T = 0$) divergences. More precisely, the leading UV divergence for $h_B(\lambda)$ in Eq. (65) comes from $g_B \simeq p$ at large p, which leads to the expression

$$h_B(\lambda) \simeq -\frac{\lambda^3}{2} \int_0^\infty dp \, p^2 \sin(\lambda p) = -\frac{1}{2} \int_0^\infty dq \, q^2 \sin(q).$$

This is formally divergent but independent of λ (and hence temperature). Any counterterm for it would have to be temperature-independent, too, but all available $T = 0$ counterterm have already been exhausted in the renormalization of the gap equation above.

There are at least three ways to deal with the spurious divergences in the functions $h(\lambda)$:
(1) Introduce a regulator $e^{-\mu p}$ in the momentum integral and perform the limit $\mu \to 0$ outside the integral;
(2) Perform integration by parts and throw away the boundary contribution from $p = \infty$;
(3) Do contour integration and throw away the large circle at complex infinity $|p| \to \infty$.

All methods are equivalent and the first two are also suitable for numerical evaluation. Let us briefly check the regulator method for the model $g(p) = p^\alpha$ with $\alpha > 0$:

$$
\begin{aligned}
h(\lambda) &= -\frac{\lambda^3}{2} \lim_{\mu \to 0} \int_0^\infty dp \, p \, \sin(\lambda p) p^\alpha e^{-\mu p}, \\
&= -\frac{\lambda}{2} \lim_{\mu \to 0} \int_0^\infty dq \, q (q/\lambda)^\alpha e^{-\mu q/\lambda} \sin q, \\
&= \lim_{\mu \to 0} -\frac{\lambda^{1-\alpha}}{2} (1 + \mu^2)^{-(1+\alpha/2)} \Gamma(\alpha + 2) \sin[(\alpha + 2) \arctan(\lambda/\mu)], \\
&= -\frac{1}{2} \lambda^{1-\alpha} \Gamma(\alpha + 2) \sin\left(\frac{\pi}{2}(\alpha + 2)\right).
\end{aligned}
\tag{89}
$$

For a free gauge boson, we have $\omega(p) = p$ and $\chi(p) = 0$ which implies $g_B(p) = p$ and thus $\alpha = 1$. In the free fermionic case, we have $M(\boldsymbol{p}) = 0$ and thus also $g_F(p) = p$ from Eq. (75). Free particles are therefore always characterized by $\alpha = 1$, which implies $h(\lambda) = 1$. This was used in the derivation of the Weiss formula above.

As a second example, take a free massive boson, $\omega(p) = g_B(p) = \sqrt{p^2 + m^2}$, and employ the integration by parts technique. We have to do four integrations by parts and drop the momentum-independent boundary terms to arrive at the finite contribution

$$
\begin{aligned}
h(\lambda) &= -\frac{1}{2\lambda} \int_0^\infty dp \, \sin(\lambda p) \frac{d^4}{dp^4}\left[p\sqrt{p^2 + m^2}\right] \\
&= \int_0^\infty dp \, \frac{15m^4 p \sin(\lambda p)}{2\lambda(p^2 + m^2)^{\frac{7}{2}}} = \frac{(m\lambda)^2}{2} K_2(m\lambda),
\end{aligned}
\tag{90}
$$

where K_2 is a modified Bessel function. In the massless limit $m \to 0$, or at high temperatures $\lambda \to 0$, we obtain again $h(0) = 1$. This can be interpreted as follows: the techniques used to derive the effective action of the Polyakov loop, Eqs. (68) and (78), can be adapted to evaluate the free energy and the pressure of thermal QCD. In that case, the same function $h(\lambda)$ appears as a multiplicative factor, and the remaining factors are such that the high temperature limit $h(0) = 1$ for each degree of freedom saturates the Stefan-Boltzmann law. Thus, the value $h(0)$ at high temperatures can be interpreted as counting the perturbative degrees of freedom as given by the Stefan-Boltzmann law [32].

In our numerical code, we have always used the regulator method explained above to deal with the spurious divergences in $h_B(\lambda)$ and $h_F(\lambda)$. Furthermore, we have always used the $T = 0$ kernels even at finite temperature. In the gluon sector, this is a standard procedure in functional methods, based on the lattice observations that the gluon propagator is only mildly affected by temperatures up to $T = 2T^*$. Furthermore, there are qualitative arguments [15] which suggest that the finite temperature corrections to the gluon kernel are of higher order in the effective potential for the gauge-invariant Polyakov loop, and it is assumed that this carries over to the present background

gauge calculation. However, a stringent proof does not exist and the justification is essentially *a posteriori*.

For the gluon sector, the Coulomb gauge propagator in both lattice [30] and variational [9] calculations can be well described by the *Gribov formula*,

$$
\omega(p) = \sqrt{p^2 + \frac{M_G^4}{p^2}},
\tag{91}
$$

with the Gribov mass $M_G \simeq 880$ MeV that sets the overall scale in the gluon sector. The curvature is then fixed by the gap equation,

$$
\chi(p) = \sqrt{-c_0 + \frac{M_G^4}{p^2}},
\tag{92}
$$

and we must have $c_0 < 0$ so that the curvature is real for all momenta. Lattice calculations indicate that these shapes are only mildly affected by finite temperatures up to $T = 2T^*$, while a corresponding calculation in the Hamiltonian approach has not yet been carried out.

In the quark sector, the solution to the gap equation (73) at $T = 0$ can be parametrized in a variety of ways, for instance

$$
M(p) = \frac{M_0}{[1 + (p/p_0)^2]^2}.
\tag{93}
$$

The mass parameters are naturally measured in units of the Coulomb string tension, $\sqrt{\sigma_C} = 695$ MeV and[5]

$$
SU(2): \quad M(0)/\sqrt{\sigma_C} = 0.143, \quad p_0/\sqrt{\sigma_C} = 0.610,
\tag{94}
$$

$$
SU(3): \quad M(0)/\sqrt{\sigma_C} = 0.190, \quad p_0/\sqrt{\sigma_C} = 0.813.
\tag{95}
$$

---

[5]We use a conservative estimate $\sigma_C = 2.5\sigma$ for the Coulomb string tension in terms of the Wilson string tension [30]. Other studies favor values up to $\sigma_C = 4\sigma$, which would mean that $\sqrt{\sigma_C} \approx M_G \approx 880$ MeV.

This is shown in Fig. 1, together with the numerical solution of the Adler-Davis equation. In the right panel, we present the resulting Fourier transform $h_F(\lambda)$ according to Eq. (77). Other fits for the mass function $M(\boldsymbol{p})$ may give a slightly better $\chi^2/\text{d.o.f.}$, but this has virtually zero impact on $h_F(\lambda)$.

Below the chiral phase transition, the quark mass function shows only a mild angular dependence caused by the violation of $O(3)$ invariance due to the heat bath [33]. This would have to be averaged over angles similarly to Eq. (66) and provides only a minor correction to the $T = 0$ form Eq. (93). Above the chiral phase transition, however, the mass function quickly vanishes for all momenta [33]. From Eq. (75), this means that $g_F(p) = p$ and hence $h_F = 1$. Recall that the argument of h_F is $\lambda = \mathfrak{m}\beta \simeq \beta$, because the $\mathfrak{m} = 1$ term dominates the Poisson sum in the potential Eq. (78) at virtually all temperatures. In the right panel of Fig. 1, λ is measured in units of $\sqrt{\sigma_C}$, so that the vanishing mass function would set $h_F = 1$ for all $\lambda \leq \sqrt{\sigma_C}/T_\chi \approx 7$, i.e. it would only slightly suppress the bump at small λ. This has, however, only a minor effect on the effective potential of the Polyakov loop at high temperatures, and none at small temperatures $T < T_\chi$. This justifies the use of the $T = 0$ solution *a posteriori*.

IV. NUMERICAL RESULTS AT 1-LOOP LEVEL

The main numerical challenge at 1-loop order is the accurate computation of the Fourier transform

$$h(\lambda) = -\frac{\lambda^3}{2} \int_0^\infty dp\, p \sin(\lambda p) g(p), \qquad (96)$$

where $g(p)$ is either $g_B(p)$ Eq. (58) or $g_F(p)$ Eq. (75) for gluons and quarks, respectively. To visualize the problem, the left panel of Fig. 2 shows the integrand in Eq. (96) as a function of the momentum p for the Gribov formula

Eq. (91) at $\lambda = 10$ and $c_0 = 0$, for a small regulator $\mu = 0.006 \ll 1$ in the extrapolation

$$h(\lambda) = -\frac{\lambda^3}{2} \lim_{\mu \to 0} \int_0^\infty dp\, p \sin(\lambda p) g(p) e^{-\mu p}. \qquad (97)$$

The numerical issue of the wildly oscillating integrand is clearly visible. Nonetheless, we have chosen to use the regulator method for our numerical code, since integration by parts may involve higher numerical derivatives, which are much less reliable. If an analytical expression for $g(p)$ is given, then we may actually take a combination of first integrating twice by parts (analytically), and then applying the regulator method, which yields the best results. The Fourier transforms can then be done to high accuracy using double exponential algorithms, combined with Richardson extrapolation to the limit $\mu \to 0$. This is shown in the right panel of Fig. 2, where the resulting transform h_B for the Gribov formula Eq. (91) is plotted as a function of the dimensionless variable $\theta = \lambda M_G$ at various regulators $\mu \ll 1$. The convergence to the limit is clearly visible but requires quite small values for μ.

Note that the scales on the horizontal axis in Figs. 1 and 2 are slightly different. Unless stated otherwise, we will nondimensionalize all quantities in the numerical code using appropriate units of the Coulomb string tension. The numerical value $\sqrt{\sigma_C} \approx 695$ MeV is then used to produce absolute numbers in various plots.

With $h_B(\lambda)$ and $h_F(\lambda)$ at hand, the computation of the effective potential of the Polyakov loop is a simple matter of summing the corresponding Poisson series, cf. Eqs. (68) and (76) for the color group $SU(2)$. Since $h_B(\lambda)$ and $h_F(\lambda)$ are bounded, the Poisson series converges at least as $1/\mathfrak{m}^4$ so that very few terms are necessary to saturate the sum, even at higher temperatures. At lower and intermediate temperatures, the first term $\mathfrak{m} = 1$ in the Poisson series gives already an accurate description, and we observe e.g. from Eq. (68) that
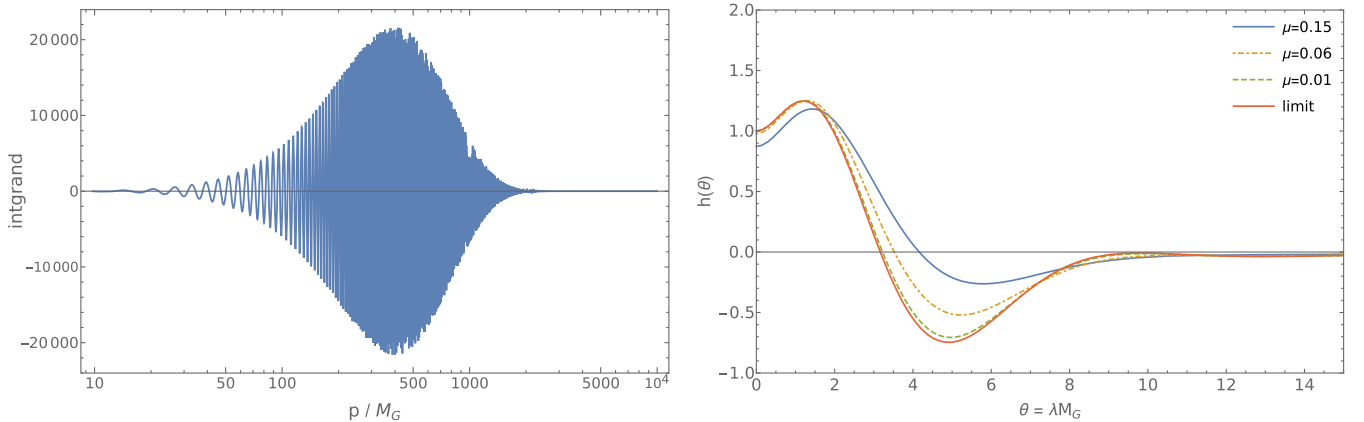

FIG. 2. Left: the integrand of the Fourier transform Eq. (96) for gluons using the Gribov formula. Right: result of the double-exponential Fourier transformation using various regulators.
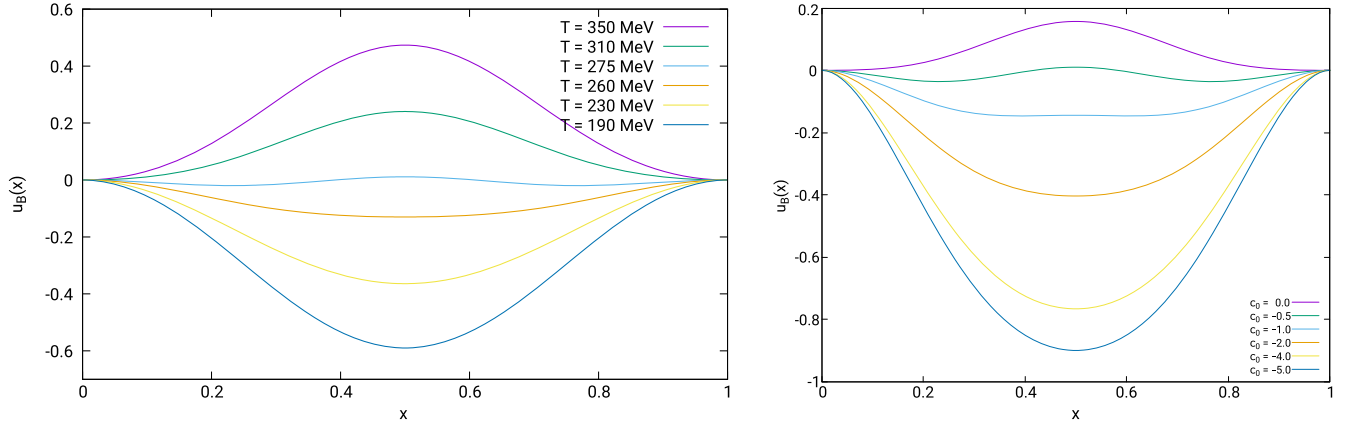
FIG. 3. Gluon part of the effective potential of the $SU(2)$ Polyakov loop for various temperatures at $c_0 = 0$ (left) and for a fixed temperature $T = 302$ MeV at various renormalization constants $c_0 \leq 0$ (right).

$$u_B(x, \beta) \approx \frac{4}{\pi^2}[1 - \cos(2\pi x)]h_B(\beta). \qquad (98)$$

This has its minimum at the center-breaking points $x \in \{0, 1\}$ if $h_B(\beta) > 0$ (deconfinement) and flips over to a minimum at the center symmetric point $x = 1/2$ (confinement) if $h_B(\beta) < 0$. The phase transition thus occurs through a sign change in the Fourier transform $h_B(\beta)$ and the critical temperature is determined by the zero, $h_B(\beta^*) = 0$. Figure 3 shows the effective potential $u_B(x)$ of the Polyakov loop Eq. (67) for various temperatures and $c_0 = 0$. In the right panel of this figure, we have plotted the potential at a fixed temperature $T = 302$ MeV for various values of $-c_0 \geq 0$. As can be seen, increasing the renormalization parameter $-c_0$ makes for a stronger confinement in the boson sector. This also increases the critical temperature T^* in the pure Yang-Mills case, because higher temperatures are necessary to overcome the strong confinement.

From the minimum x^* of the Polyakov loop potential, we can compute the expectation value of the Polyakov loop itself through

$$SU(2): \quad \langle L \rangle = \frac{1}{2}\mathrm{tr}\,\exp\left(-\beta a_3^* \sigma_3/2i\right) = \cos(\pi x^*), \quad (99)$$

$$SU(3): \quad \langle L \rangle = \frac{1}{3}\mathrm{tr}\,\exp\left(-\beta a_3^* \lambda_3/2i - \beta a_8^* \lambda_8/2i\right)$$
$$= \frac{1}{3}\sqrt{1 + 4\cos(\pi x^*)[\cos(\pi x^*) + \cos(2\pi y^*/\sqrt{3})]}. \qquad (100)$$

The result is plotted for $c_0 = 0$ in Fig. 4. We observe the well-known second order phase transition for $G = SU(2)$ at a critical temperature of $T^* \approx 266$ MeV, while the transition is first order for $G = SU(3)$ with a critical temperature of $T^* \approx 278$ MeV.

As explained earlier, increasing the renormalization parameter $-c_0$ makes for a stronger gluon confinement, i.e. the critical temperature in the pure Yang-Mills case increases. This can be seen in Fig. 5 where the Polyakov loop is plotted at various values of c_0. The critical temperature measured on the lattice [14] for $G = SU(2)$ is $T^* = 306$ MeV, which indicates that a value in the range
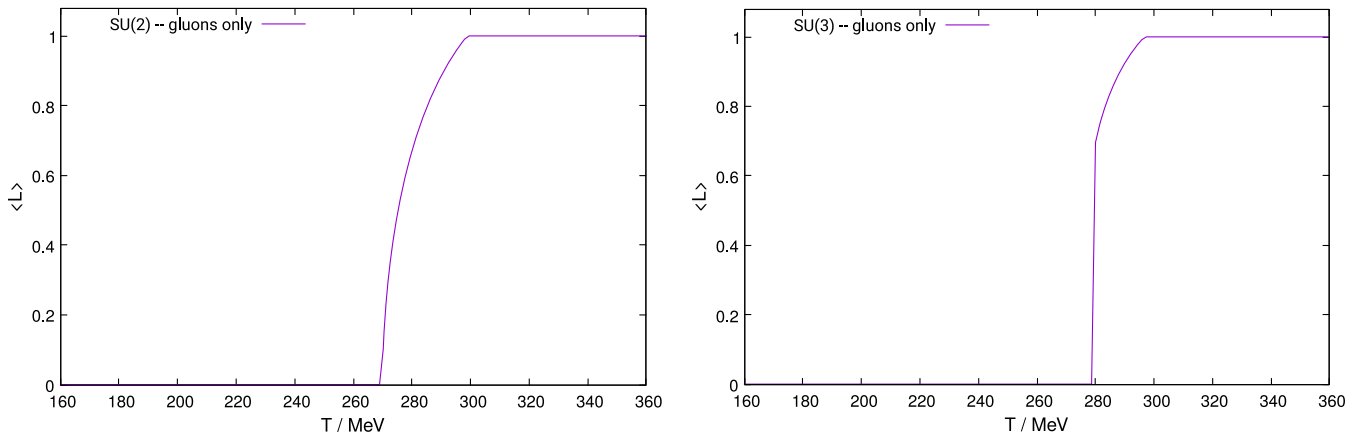

FIG. 4. The bosonic contribution to the Polyakov loop at 1-loop level, as a function of temperature, for the standard renormalization constant $c_0 = 0$. The left panel is for $SU(2)$, and the right panel is for $SU(3)$.
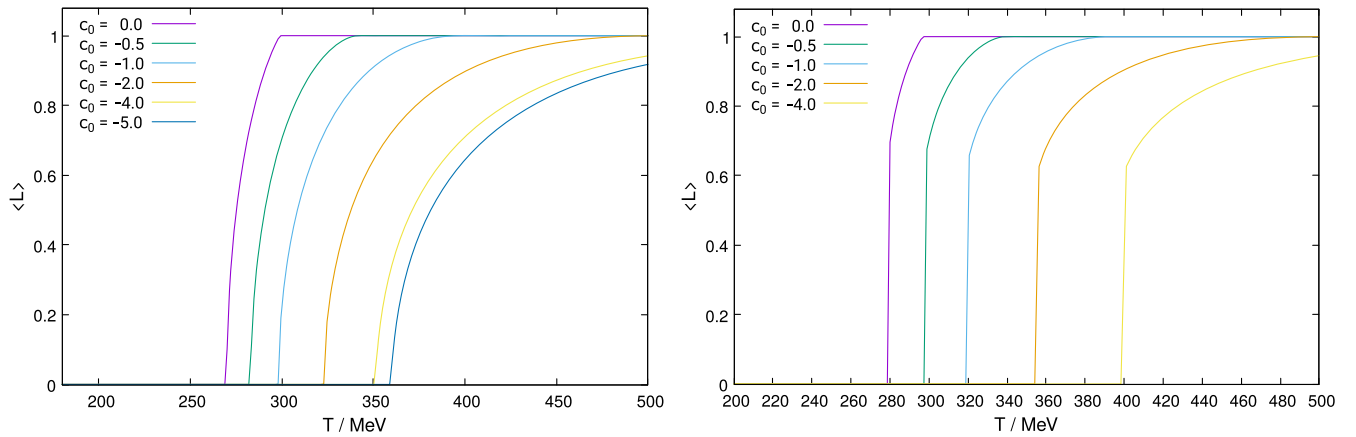
FIG. 5.   The bosonic contribution to the Polyakov loop at 1-loop level as a function of temperature, for various values of the renormalization parameter c_0. The left panel is for $G = SU(2)$, and the right panel is for $G = SU(3)$.

$-c_0 \simeq 1.0\ldots2.0$ is compatible with the lattice and describes the transition at least as well as the standard choice $c_0 = 0$. For $G = SU(3)$ shown in the right panel of Fig. 5, the agreement with the lattice favors the standard value $c_0 = 0$, but the good agreement with the transition temperature $T^* \approx 278$ MeV on the lattice [14] must be considered accidental given our approximations. Within the expected accuracy of our calculation, values up to $c_0 \simeq -1.5$ are still compatible with the lattice findings. The bottom line is that the acceptable range for the renormalization parameter c_0 is, for both color groups, about $c_0 \in [-1.5, \ldots, 0]$, and the value $c_0 = 0$ used in earlier studies is usually preferred, at least for $SU(3)$.

Next, let us include the fermion contribution at 1-loop level. Numerically, the calculation of the quark contribution is very similar to the gluon case, with the mass function $M(p)$ entering first the function $g_F(p)$ in Eq. (75), which is then Fourier transformed, using the techniques described earlier, into the profile function $h_F(\lambda)$ in Eq. (77). This function plays a similar role as in the boson case: it

provides a profile prefactor $h_F(\beta)$ for the dominant term in the effective potential of the Polyakov loop, Eqs. (78) and (80). The positive sign of h_F in Fig. 1 thus indicates deconfinement at all temperatures, which is expected on physical grounds: quarks should turn the phase transition into a soft *crossover* while leaving confinement intact at small temperatures below the dynamical quark mass.

Surprisingly, these reasonable expectations are *not* fully met at 1-loop level, as can be seen in Fig. 6: while the transition is indeed softened into a crossover, the quarks start to dominate at temperatures below $T^*/2$, so that the confinement eventually breaks down and the Polyakov loop approaches $\langle L \rangle = 1$ again. This occurs in the same way for both color groups $SU(2)$ and $SU(3)$. The situation becomes even worse when the number N_f of (light) quark flavors is increased.

To understand the physics behind these unexpected findings, consider the gluon 1-loop contribution to the effective potential, Eq. (98). As explained in the paragraph after Eq. (98) confinement is a consequence of a negative sign
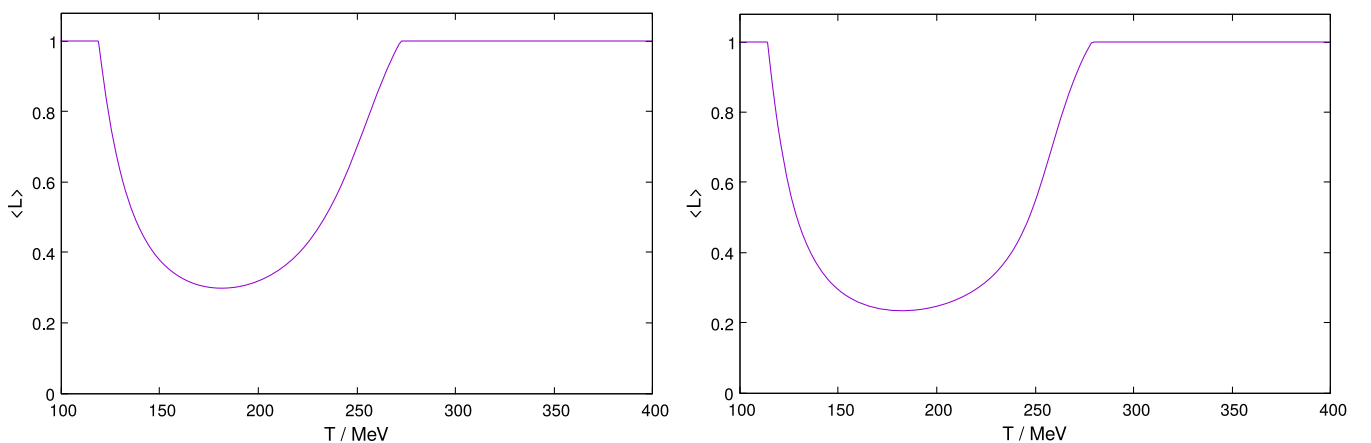

FIG. 6.   The 1-loop contribution to the Polyakov loop in full QCD as a function of temperature for $N_f = 1$ and $c_0 = 0$. The left panel is for $G = SU(2)$, and the right panel is for $G = SU(3)$.

in $h_B(\beta)$, which effectively flips the shape of the effective potential. From our discussion of the profile h_B in Sec. III C, we also know that this quantity essentially measures the number of active massless particles in the spectrum, in the sense that each free massless particle contributes $(+1)$ to h_B (ghosts contribute with a negative sign). This is the basis of the confinement mechanism in covariant functional approaches [5,7,15,16,22,34–38]: Perturbatively, there are three covariantly transversal gluon modes, one massless longitudinal mode which decouples from the dynamics, and two ghost degrees of freedom, for a total of $3 + 1 - 2 = 2 > 0$, which is reflected in $h_B \to 2$ at high temperatures. As we lower the temperature, the three transversal modes become massive through interactions and eventually decouple, so that the mode count is $0 + 1 - 2 = -1 < 0$. We now have $h_B \to -1$ and hence confinement. The salient point here is that confinement is caused predominantly by the ghost degrees of freedom and this makes for a very *strong* confinement, which cannot be overcome by quarks at low temperature, since the quarks become massive at $\beta \to \infty$ and hence tend to $h_F \to +0$, cf. Fig. 1. The quarks thus soften the transition, but cannot overcome the strong confinement caused by *ghost dominance*.

By contrast, the Hamiltonian approach predicts a profile $h_B(\beta)$ which is strongly negative (confining) at intermediate temperatures, but approaches $h_B \to -0$ at low temperatures (large λ), cf. Fig. 2. This means that the 1-loop confinement in the Hamiltonian approach to Yang-Mills theory is actually very *weak* or *fragile* at low temperatures. This fragility does *not* show up in the Polyakov loop, because the effective potential still attains its tiny negative minimum at $x = \frac{1}{2}$, so that $\langle L \rangle = 1$. However, even the smallest deconfining effect, such as $N_f = 1$ flavor of quarks, can overcome the weak confinement.

The Hamiltonian approach has only physical (transversal) gluon modes, and there is no trace of ghost dominance at small temperatures. In fact, the ghosts tend to nullify the strong gluon confinement induced by the Gribov propagator, which can be seen directly from Eq. (50): without the curvature, confinement would be strong, actually *too* strong as the transition temperature would increase to unreasonable values. There is hence a *ghost compensation* rather than a *ghost dominance* at the 1-loop level in the Hamiltonian approach, and the confining phase is essentially devoid of light degrees of freedom. This leads to problems with confinement, but it may actually be closer to the true physical picture: in the ghost dominance scenario, the abundance of massless ghost particles leads to unphysical results for most thermodynamic quantities such as a remanent pressure or a negative energy density below the phase transition [32]. This happens because the true physical picture is an exponentially suppressed partition function and a vanishing pressure, as the lightest colorless glueball excitation has a mass of well above 1 GeV. A vacuum of suppressed (compensated) excitations, as in the Hamiltonian approach, is hence not completely without physical merits.

Still, we need to fully understand the mechanism of how confinement comes about in the Hamiltonian approach. Modifications to the quark sector such as explicit coupling to gluons in the variational *Ansatz* will not change the physical picture qualitatively—quarks will still be deconfining and $h_F \to +0$ at low temperatures. The real cause of the problem is not the strength of the quark deconfinement but rather the weakness of the gluon confinement. This can be seen when improving the confining strength through the undetermined counterterm c_0, cf. Fig. 7. As can be clearly seen, all curves with $c_0 < 0$ tend to $\langle L \rangle \to 0$ at very small temperatures. Thus, even a very small perturbation of the delicate balance between gluons and ghosts through the counterterm $c_0 < 0$ is sufficient to eventually restore confinement. This indicates that the inclusion of 2-loop gluon contributions, though mostly irrelevant for the gap equation, may just give sufficient contributions to the gluon energy to restore enough gluon confinement for a decent
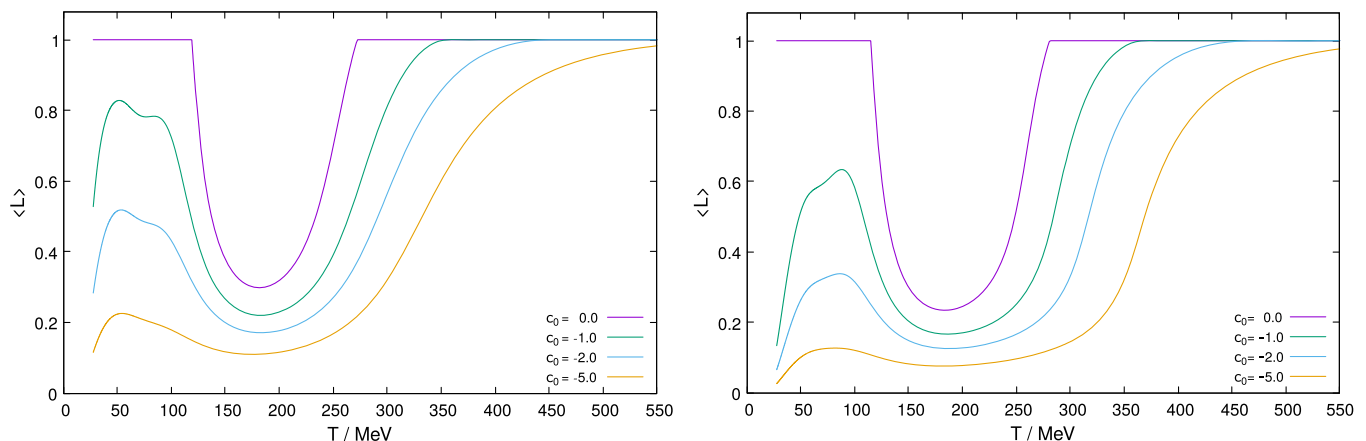

FIG. 7. The Polyakov loop in full QCD including all 1-loop contributions, for $N_f = 1$ flavors and various values of the renormalization parameter c_0. The left panel is for $SU(2)$ and the right panel for $SU(3)$.

physical picture. In the next section, we will therefore study the qualitative effects of the gluon 2-loop contributions to the effective action of the Polyakov loop.[6]

V. GLUON 2-LOOP CONTRIBUTIONS

In the previous sections, we have repeatedly stressed that the gap equation mixes loop orders, and the self-consistent 1-loop contribution to the energy actually contains parts of the 2-loop terms. This rises the question whether the self consistent 2-loop contribution must be corrected to avoid double counting. As explained in Appendix B, the 2-loop energy E_2 (valid for *all* kernels) *differs* from the self-consistent 2-loop energy E_2^{sc} (valid only for solutions of the gap equation) by a subtraction which compensates for the 2-loop terms moved from E_2 into E_1^{sc} via the gap equation. In other words, $E_1 + E_2 = E_1^{\text{sc}} + E_2^{\text{sc}}$ for solutions of the gap equation, and we must use E_2^{sc} if we also used the self-consistent 1-loop energy, and E_2 otherwise.

In our present investigation, this subtlety does not matter: the only 2-loop term included in the gap equation is the $T = 0$ contribution c_0 from the tadpole term, i.e. the non-Abelian magnetic field. (We do not include the Coulomb term or any finite temperature corrections to the gap equation.) This means that the self-consistency correction must only be applied to this particular 2-loop term. As further explained in Appendix B, the correction is substantial and would actually flip the sign of the $T = 0$ tadpole in $e_B[a]$. Since the contribution is, however, independent of temperature and the background field, it drops out when computing the Polyakov loop from the *change* in the energy, $e_B[a] - e_B[0]$. The bottom line is hence that $E_2 = E_2^{\text{sc}}$ in the present study, and no self-consistency correction should be applied to any 2-loop term.

A. The non-Abelian magnetic energy

From Eq. (39), there are two 2-loop contributions to the gluon sector. In the present subsection, we first study the term arising from the non-Abelian part of the color magnetic field,

$$\langle H_{\text{YM}}^{\text{NA}}\rangle_{\mathsf{a}} = \left\langle \frac{1}{4g^2}\int d^4x [A_i(\boldsymbol{x}), A_k(\boldsymbol{x})][A_i(\boldsymbol{x}), A_k(\boldsymbol{x})]\right\rangle_{\mathsf{a}}. \tag{101}$$

Since our trial wave functional Eq. (19) in the bosonic sector is Gaussian, Wick's theorem entails

---

[6]Recall that c_0 is the finite part of the counterterm to the non-Abelian magnetic energy, which is a 2-loop contribution. There is also a 2-loop contribution to the quark sector from the Coulomb term in Eq. (40). It has partially been included in our fermion 1-loop calculation through the self-interaction in the gap equation, and is not expected to contribute to the solution of the weak gluon confinement. We therefore defer its study to a future investigation.

$$\langle H_{\text{YM}}^{\text{NA}}\rangle_{\mathsf{a}} = \frac{f^{eab}f^{ecd}}{4g^2}\int d^3x [D_{ik}^{ab}(\boldsymbol{x},\boldsymbol{x})D_{ik}^{cd}(\boldsymbol{x},\boldsymbol{x}) \\ + D_{ii}^{ac}(\boldsymbol{x})D_{kk}^{bd}(\boldsymbol{x}) + D_{ik}^{ad}(\boldsymbol{x},\boldsymbol{x})D_{ki}^{bc}(\boldsymbol{x},\boldsymbol{x})], \tag{102}$$

where $D_{ik}^{ab}(\boldsymbol{x},\boldsymbol{y}) = \langle A_i^a(\boldsymbol{x})A_k^b(\boldsymbol{y})\rangle_{\mathsf{a}}$ is the gluon propagator in the presence of a background field, and f^{abc} are the structure coefficients of the color algebra.

Let us first consider the case $T = 0$ without a background field. Global color and Lorentz invariance implies that the gluon propagator is color diagonal and transversal in this case, i.e. we have in momentum space $D_{ik}^{ab}(\boldsymbol{p}) = \delta^{ab} t_{ik}(p)D(p)$. With our trial wave functional (19), the propagator is $D(p) = g^2/[2\omega(p)]$ in terms of the variational kernel $\omega(p)$. We note in passing that the first term in Eq. (102) vanishes due to the color symmetry of the propagator. For the remaining terms, it is easy to work out the color and Lorentz traces which result in

$$\langle H_{\text{YM}}^{\text{NA}}\rangle_0 = \frac{N(N^2-1)}{16}g^2 V_3\int\frac{d^3p}{(2\pi)^3}\int\frac{d^3q}{(2\pi)^3}\frac{3-(\hat{p}\,\hat{q})^2}{\omega(p)\omega(q)}. \tag{103}$$

The gap equation follows from the variation of the energy functional with respect to the gluon propagator. For the non-Abelian magnetic energy, this yields

$$\frac{\delta}{\delta\omega(k)^{-1}}\langle H_{\text{YM}}^{\text{NA}}\rangle_0 = \frac{N^2-1}{2(2\pi)^3}V_3\cdot\frac{Ng^2}{4}\int\frac{d^3q}{(2\pi)^3}\frac{3-(\hat{k}\,\hat{q})^2}{\omega(q)}. \tag{104}$$

Note that we have pulled out a prefactor which is common to all contributions to the gap equation, cf. Eq. (B2). To renormalize Eq. (104), we must add the mass counterterm (82) to the original Hamiltonian. Its contribution to the total energy can also be evaluated by Wick's theorem,

$$\langle H_{\text{ct}}\rangle_0 = \frac{C_0}{2g^2}\cdot 2(N^2-1)V_3\int\frac{d^3q}{(2\pi)^3}D(q) \\ = \frac{N^2-1}{2}V_3 C_0\int\frac{d^3q}{(2\pi)^3}\frac{1}{\omega(q)}. \tag{105}$$

The variation with respect to the gluon propagator gives a constant

$$\frac{\delta}{\delta\omega(k)^{-1}}\langle H_{\text{ct}}\rangle_0 = \frac{N^2-1}{2(2\pi)^3}V_3\cdot C_0. \tag{106}$$

We note that the same prefactor as in Eq. (104) has appeared. The condition that the counterterm cancels the divergence in Eq. (104) is satisfied if C_0 depends on the cutoff (not the momentum) in such a way that[7]

---

[7]After the angular integration, the loop integral is independent of the external momentum k and depends only on the UV cutoff Λ.

$$c_0 \equiv C_0 + \frac{Ng^2}{4} \int \frac{d^3q}{(2\pi)^3} \frac{3 - (\hat{k}\,\hat{q})^2}{\omega(q)} \qquad (107)$$

is finite. The finite coefficient c_0 is precisely the renormalization parameter of the same name introduced earlier in Eq. (85) of the previous section.

We will now show that Eq. (107) is also sufficient to render the entire non-Abelian magnetic energy finite, even in the presence of a background field and at finite temperature. The modifications to the non-Abelian magnetic energy Eq. (103) necessary to account for finite temperature and a constant background field in the Cartan subalgebra follow the techniques described at length in Sec. III: we introduce finite temperatures in the loop integrals by compactifying the (spatial) direction of the heat bath. Furthermore, we replace the color trace by a sum over all roots and note that the constant background in the Cartan subalgebra only enters via the covariant derivative. After Fourier transformation, this amounts to (i) replacing the integration in the direction of the heat bath by a Matsubara sum and (ii) shifting the momentum arguments in the kernels $\boldsymbol{p} \to \boldsymbol{p}^\sigma$ as in Eq. (29). After Poisson resumming the Matsubara sum and shifting the loop integration, we end up with

$$\langle H_{\mathrm{YM}}^{\mathrm{NA}} \rangle_{\mathsf{a}} = \frac{g^2}{16} V_2 \beta \int \frac{d^3p}{(2\pi)^3} \int \frac{d^3q}{(2\pi)^3} \frac{3 - (\hat{p}\,\hat{q})^2}{\omega(p)\omega(q)}$$
$$\times \sum_{\rho,\sigma,\tau} |f_{\rho,\sigma,\tau}|^2 \sum_{\mathfrak{n}=-\infty}^{\infty} \exp[i\mathfrak{n}\beta(q_3 + \underline{\sigma} \cdot \underline{\mathsf{a}})]$$
$$\times \sum_{\mathfrak{m}=-\infty}^{\infty} \exp[i\mathfrak{m}\beta(q_3 + \underline{\tau} \cdot \underline{\mathsf{a}})]. \qquad (108)$$

For the simple case of the color group $SU(2)$, the structure constants $f_{\rho,\sigma,\tau}$ in the Cartan basis read

$$f_{\rho,\sigma,\tau} = \epsilon_{\rho\sigma\tau} = \{\epsilon_{-1,0,1} = 1 \,\mathrm{and}\,\mathrm{cyclic}\}, \quad \rho,\sigma,\tau \in \{-1,0,1\}. \qquad (109)$$

Further details can be found in Appendix A. For all color groups $SU(N)$ we have $|f_{\rho,\sigma,\tau}|^2 = N(N^2 - 1)$ when summed over all roots. This shows that the $\mathfrak{m} = \mathfrak{n} = 0$ term in Eq. (109) agrees with the $T = 0$ vacuum contribution Eq. (103). This term is independent of the background field and will drop out once the change of the free energy due to the background is considered, cf. Eq. (55). Of the remaining terms, only the ones are singular in which one of the two Poisson indices vanishes. (This is intuitively clear, but the proof is rather technical and thus deferred to Appendix C.)

Using Eq. (A6) for the color trace, the singular terms in Eq. (108) read

$$\langle H_{\mathrm{YM}}^{\mathrm{NA}} \rangle_{\mathsf{a}}\big|_{\mathrm{sing}} = 2N \frac{g^2}{16} \beta V_2 \int \frac{d^3p}{(2\pi)^3} \int \frac{d^3q}{(2\pi)^3} \frac{3 - (\hat{p}\,\hat{q})^2}{\omega(p)\omega(q)}$$
$$\times \sum_{\substack{\mathfrak{m}=-\infty \\ \mathfrak{m}\neq 0}}^{\infty} \sum_{\sigma} \exp[i\mathfrak{m}\beta(q_3 + \underline{\sigma} \cdot \underline{\mathsf{a}})]. \qquad (110)$$

By the same technique, the counterterm H_{ct} Eq. (82) contributes, at finite temperature and in the presence of a background field,

$$\langle H_{\mathrm{ct}} \rangle_{\mathsf{a}} = \frac{C_0}{2} \beta V_2 \int \frac{d^3q}{(2\pi)^3} \frac{1}{\omega(q)} \sum_{\mathfrak{m}=-\infty}^{\infty}$$
$$\times \sum_{\sigma} \exp[i\mathfrak{m}\beta(q_3 + \underline{\sigma} \cdot \underline{\mathsf{a}})]. \qquad (111)$$

The $\mathfrak{m} = 0$ vacuum contribution of this expression cancels the divergence in the vacuum contribution of the non-Abelian magnetic energy, cf. Eq. (107). These terms would, however, drop out anyhow when computing the effective potential of the Polyakov loop. In addition, however, the $T = 0$ renormalization (107) is also sufficient to cancel all UV divergences in the finite temperature corrections, as can be seen explicitly from Eqs. (110) and (111). The combination of these two expression gives the finite contribution

$$\langle H_{\mathrm{YM}}^{\mathrm{NA}} \rangle_{\mathsf{a}}\big|_{\mathrm{sing,ren}} = \frac{c_0}{2} \beta V_2 \int \frac{d^3q}{(2\pi)^3} \frac{1}{\omega(q)} \sum_{\substack{\mathfrak{m}=-\infty \\ \mathfrak{m}\neq 0}}^{\infty}$$
$$\times \sum_{\sigma} \exp[i\mathfrak{m}\beta(q_3 + \underline{\sigma} \cdot \underline{\mathsf{a}})]. \qquad (112)$$

This is again a 1-loop term which now depends *explicitly* on the renormalization constant c_0. (In Sec. III, the dependency on c_0 was only indirect via the curvature computed from the gap equation.) To complete the non-Abelian magnetic field, we must also add the finite 2-loop contribution from the terms $(\mathfrak{m} \neq 0, \mathfrak{n} \neq 0)$ in Eq. (108). The techniques used to treat these terms numerically are identical for the Coulomb contribution studied in the next section, and we defer the details to Sec. V C below.

B. The gluon part of the Coulomb potential

The last term in Eq. (39) is the contribution of the non-Abelian Coulomb term to the gluon energy, i.e. the expectation value of Eq. (15) in the gluon sector,

$$\langle H_C^A \rangle_{\mathsf{a}} = \frac{g^2}{2} \int d^3(x,y) \langle \mathcal{J}_{\mathsf{a}}^{-1}[A] \rho_{\mathrm{YM}}^a(\boldsymbol{x}) \mathcal{J}_{\mathsf{a}}[A] \hat{F}^{ab}(\boldsymbol{x},\boldsymbol{y}) \rho_{\mathrm{YM}}^b \rangle_{\mathsf{a}}, \qquad (113)$$

where the gluon color charge $\rho_{\mathrm{YM}}^a(\boldsymbol{x}) = f^{abc} A_k^b(\boldsymbol{x}) \Pi_k^c(\boldsymbol{x})$ now contains a functional derivative, $\boldsymbol{\Pi}(\boldsymbol{x}) = -i\delta/\delta \boldsymbol{A}(\boldsymbol{x})$. The expectation value in Eq. (113) implies that the integrand should be sandwiched between two trial wave

functionals. It is then convenient to functionally integrate by parts and let the derivative in the left factor ρ_{YM} act on the wave function to the left, and the right factor ρ_{YM} act to the right:

$$-\frac{\delta}{\delta A_k^a(x)}\left[\mathcal{J}_a[A]^{-\frac{1}{2}}\exp\left(-\frac{1}{2g^2}\int(A-a)\omega(A-a)\right)\right]$$
$$= E_k^a(x)\cdot\mathcal{J}_a[A]^{-\frac{1}{2}}\exp\left(-\frac{1}{2g^2}\int(A-a)\omega(A-a)\right).$$

The factor E can be interpreted as an electric field and reads explicitly:

$$E_i^a(x)=\frac{1}{g^2}\left[\int dy\,\hat{\omega}_{ik}^{ab}(x,y)(A-a)_k^b(y)+\frac{g^2}{2}\frac{\delta\ln\mathcal{J}_a[A]}{\delta A_i^a(x)}\right].$$
(114)

The Coulomb energy can now be recast to

$$\langle H_C^A\rangle_a=\frac{g^2}{2}\int d^3(x,y)\langle f^{acd}A_i^c(x)E_i^c(x)\cdot\hat{F}^{ab}(x,y)$$
$$\cdot f^{bc'd'}A_k^{c'}(y)E_k^{c'}(y)\rangle_a.$$
(115)

To proceed, we use the curvature approximation for the Faddeev-Popov determinant [9] in the presence of a background field,

$$\left\langle\frac{g^2}{2}\frac{\delta\ln\mathcal{J}_a[A]}{\delta A_i^a(x)}\cdots\right\rangle_a\approx\left\langle\int dy\,\hat{\chi}_{ik}^{ab}(x,y)(A-a)_k^b(y)\cdots\right\rangle_a,$$
(116)

which is valid to the given order, but only under the expectation value. The electric field now simplifies considerably,

$$E_i^a(x)\approx\frac{1}{g^2}\int dy\,[\hat{\omega}-\hat{\chi}]_{ik}^{ab}(x,y)(A-a)_k^b(y).$$
(117)

Furthermore, we can also factorize the expectation value in Eq. (115) to the given order,

$$\langle H_C^A\rangle_a\approx\frac{1}{2}\int d^3(x,y)\langle f^{acd}A_i^c(x)E_i^c(x)$$
$$\cdot f^{bc'd'}A_k^{c'}(y)E_k^{c'}(y)\rangle_a\cdot\langle g^2\hat{F}^{ab}(x,y)\rangle_a.$$
(118)

Here, the second expectation value is the non-Abelian Coulomb potential,[8]

$$\langle g^2\hat{F}^{ab}(x,y)\rangle_a\approx\langle g^2\hat{F}^{ab}(x,y)\rangle_0=\delta^{ab}V_C(x-y).$$
(119)

This potential has already been used in the Fermi sector. We can model its long-ranged part, as obtained from variational calculations in the Yang-Mills sector or the lattice, by a linear rising potential, $V_C=-\sigma_C|x-y|$. In momentum space, this amounts to $V_C(p)=8\pi\sigma_C/p^4$, cf. Sec. III B.

With Eq. (117), the operator in the first expectation value in Eq. (118) reduces to a monomial in the gauge field, which can be evaluated using Wick's theorem. The presence of the background field in our trial wave functional implies that the contractions are only color diagonal when the Cartan basis is used (cf. Appendix A),

$$\langle A_i^a(x)A_k^b(y)\rangle_a=D_{ik}^{ab}(x,y)=\langle a|\sigma\rangle D_{ik}^\sigma(x,y)\langle\sigma|b\rangle.$$

We must also introduce finite temperature by compactifying the 3-axis, Fourier transform and Poisson resum the Matsubara series. After a lengthy but straightforward calculation along the lines laid out earlier, we arrive at

$$\langle H_C^A\rangle_a=\frac{g^2}{2}V_2\beta\sum_{\sigma,\rho,\tau}|f_{\sigma,\rho,\tau}|^2\int\frac{d^3p}{(2\pi)^3}\int\frac{d^3p}{(2\pi)^3}F(q+p-e_3\underline{a}(\underline{\sigma}+\underline{\tau}+\underline{\rho}))\tilde{f}(p,q)$$
$$\times\sum_{\mathfrak{n}\in\mathbb{Z}}\exp[i\mathfrak{n}\beta(p_z+\underline{a}\cdot\underline{\sigma})]\sum_{\mathfrak{m}\in\mathbb{Z}}\exp[i\mathfrak{m}\beta(q_z+\underline{a}\cdot\underline{\tau})].$$
(120)

Here, the contractions give rise to the function

$$\tilde{f}(p,q)=[\omega(p)D(p)\omega(p)]_{ij}D(q)_{ji}$$
$$-[\omega(p)D(p)]_{ij}[\omega(q)D(q)]_{ji}$$

in the integrand. Furthermore, the shift in the momentum argument of the Coulomb potential is due to the background field expectation value, cf. Eq. (119). For any

function of the root vectors, $\phi(\underline{\sigma})$, we have the relation (no sum over repeated indices)

$$|f_{\rho,\sigma,\tau}|^2\phi(\underline{\rho}+\underline{\sigma}+\underline{\tau})=|f_{\rho,\sigma,\tau}|^2\phi(\underline{0}),$$
(121)

because the structure constants are only nonzero for such combination of roots for which the sum of the root vectors vanish. This entails that the momentum shift in the Coulomb potential can actually be omitted, which explains the first equality in Eq. (119). Putting everything together and dividing by the space volume βV_2, the contribution of the Coulomb term to the energy density becomes

---

[8]The first equality will be explained in Eq. (121) below.

$$e_C[\mathsf{a}] = \frac{1}{8}\sum_{\rho,\sigma,\tau}|f_{\sigma,\rho,\tau}|^2 \int \frac{d^3p}{(2\pi)^3}\int \frac{d^3p}{(2\pi)^3}V_C(\boldsymbol{p}+\boldsymbol{q})[1+(\hat{\boldsymbol{p}}\cdot\hat{\boldsymbol{q}})^2]f(\boldsymbol{p},\boldsymbol{q})$$

$$\times \sum_{\mathfrak{n}\in\mathbb{Z}}\exp[i\mathfrak{n}\beta(p_z+\underline{\mathsf{a}}\cdot\underline{\sigma})]\sum_{\mathfrak{m}\in\mathbb{Z}}\exp[i\mathfrak{m}\beta(q_z+\underline{\mathsf{a}}\cdot\underline{\tau})], \tag{122}$$

where the variation kernels appear only in the scalar function

$$f(\boldsymbol{p},\boldsymbol{q}) = \frac{\Omega(\boldsymbol{p})[\Omega(\boldsymbol{p})-\Omega(\boldsymbol{q})]}{\omega(\boldsymbol{p})\omega(\boldsymbol{q})}, \quad \text{with} \quad \Omega(\boldsymbol{p})\equiv\omega(\boldsymbol{p})-\chi(\boldsymbol{p}). \tag{123}$$

From the structure of Eq. (122), it is clear that $f(\boldsymbol{p},\boldsymbol{q})$ can be symmetrized under the integral,

$$f(\boldsymbol{p},\boldsymbol{q}) = \frac{1}{2}\frac{[\Omega(\boldsymbol{p})-\Omega(\boldsymbol{q})]^2}{\omega(\boldsymbol{p})\omega(\boldsymbol{q})}, \tag{124}$$

which is more convenient. The final form Eq. (122) of the Coulomb contribution has the same mathematical structure as the non-Abelian magnetic energy in Eq. (108). This allows us to use the same analysis and numerical technique in both cases. We will describe our method briefly in the next subsection.

C. General computation of 2-loop terms

Both 2-loop contributions (108) and (122) to the gluon energy density have the same general form in the presence of a background field and at finite temperature,

$$e[\mathsf{a}] = \int \frac{d^3p}{(2\pi)^3}\int \frac{d^3q}{(2\pi)^3}\sum_{\rho,\sigma,\tau}|f_{\rho,\sigma,\tau}|^2\phi(\boldsymbol{p},\boldsymbol{q})$$

$$\times \sum_{\mathfrak{m}=-\infty}^{\infty}e^{i\mathfrak{m}\beta(p_z+\underline{\mathsf{a}}\cdot\underline{\sigma})}\sum_{\mathfrak{n}=-\infty}^{\infty}e^{i\mathfrak{n}\beta(q_z+\underline{\mathsf{a}}\cdot\underline{\tau})}, \tag{125}$$

where the symmetric function $\phi(\boldsymbol{p},\boldsymbol{q})$ contains the variation kernels. For simplicity, we will limit the following considerations to the color group $G=SU(2)$ and also make use of some explicit properties of the $SU(2)$ Cartan base; the generalization to $G=SU(N)$ will be studied elsewhere.

We begin by collecting all factors in the integrand that depend on the background field a. For $G=SU(2)$, the roots are scalar numbers from $\{-1,0,1\}$, and the background field is also a scalar $\underline{\mathsf{a}}=\mathsf{a}$. Using $f_{\rho,\sigma,\tau}=\epsilon_{\rho\sigma\tau}$ and working out the color trace yields

$$\sum_{\rho,\sigma,\tau}|f_{\rho,\sigma,\tau}|^2 e^{i\beta\underline{\mathsf{a}}\cdot(\mathfrak{m}\underline{\sigma}+\mathfrak{n}\underline{\tau})} = \sum_{\sigma=\pm1}[e^{i\beta\mathsf{a}\sigma(\mathfrak{m}-\mathfrak{n})}+e^{i\beta\sigma\mathfrak{a}\mathfrak{n}}+e^{i\beta\sigma\mathfrak{a}\mathfrak{m}}]. \tag{126}$$

When inserting the last term on the rhs of Eq. (126) back into Eq. (125), the result can be put in the form

$$\int \frac{d^3p}{(2\pi)^3}\sum_{\mathfrak{m}=-\infty}^{\infty}\sum_{\sigma=\pm1}e^{i\mathfrak{m}\beta(p_z+\sigma\mathsf{a})}\cdot g(\boldsymbol{p},\beta), \tag{127}$$

where the function

$$g(\boldsymbol{p},\beta) = \int \frac{d^3q}{(2\pi)^3}\phi(\boldsymbol{p},\boldsymbol{q})\sum_{\mathfrak{n}=-\infty}^{\infty}e^{i\mathfrak{n}\beta q_z} \tag{128}$$

depends on the temperature, but not on the background field a. By relabeling $\mathfrak{m}\leftrightarrow\mathfrak{n}$ and $\boldsymbol{p}\leftrightarrow\boldsymbol{q}$, it is easily seen that the second contribution on the rhs of Eq. (126) yields the same result, with the arguments in $\phi(\boldsymbol{p},\boldsymbol{q})$ reversed (which is irrelevant, as ϕ can be assumed symmetric).

The first term on the rhs of Eq. (126) is a bit more involved. Inserting it in Eq. (125) yields

$$\int \frac{d^3p}{(2\pi)^3}\int \frac{d^3q}{(2\pi)^3}\phi(\boldsymbol{p},\boldsymbol{q})\sum_{\mathfrak{m}=-\infty}^{\infty}\sum_{\mathfrak{n}=-\infty}^{\infty}$$

$$\times \sum_{\sigma=\pm1}e^{i\mathfrak{m}\beta p_z+i\mathfrak{n}\beta q_z+i\beta(\mathfrak{m}-\mathfrak{n})\sigma\mathsf{a}}.$$

If the Poisson series and the loop integration _were_ absolutely convergent, we could shift the summation index $\mathfrak{m}\to\ell=\mathfrak{m}-\mathfrak{n}$ and the integration variable $\boldsymbol{q}\to\boldsymbol{q}'=\boldsymbol{q}+\boldsymbol{p}$ to coerce the contribution in the form Eq. (127). After renaming again $\ell\to\mathfrak{m}$ and $\boldsymbol{q}'\to\boldsymbol{q}$, we would again find the form Eq. (127) with[9]

$$g(\boldsymbol{p},\beta) = \int \frac{d^3q}{(2\pi)^3}\phi(\boldsymbol{p},\boldsymbol{q}-\boldsymbol{p})\sum_{\mathfrak{n}=-\infty}^{\infty}e^{i\mathfrak{n}\beta q_z}. \tag{129}$$

Collecting all pieces gives the energy density in the form

$$e[\mathsf{a}] = \int \frac{d^3p}{(2\pi)^3}\sum_{\mathfrak{m}=-\infty}^{\infty}\sum_{\sigma=\pm1}e^{i\mathfrak{m}\beta(p_z+\sigma\mathsf{a})}\cdot g(\boldsymbol{p},\beta), \tag{130}$$

$$g(\boldsymbol{p},\beta) = \int \frac{d^3q}{(2\pi)^3}\sum_{\mathfrak{n}=-\infty}^{\infty}e^{i\mathfrak{n}\beta q_z}\Big[\phi(\boldsymbol{p},\boldsymbol{q})+\phi(\boldsymbol{q},\boldsymbol{p})$$

$$+\frac{1}{2}\phi(\boldsymbol{p},\boldsymbol{q}-\boldsymbol{p})+\frac{1}{2}\phi(\boldsymbol{q}-\boldsymbol{p},\boldsymbol{p})\Big]. \tag{131}$$

---

[9]Shifting instead $\boldsymbol{p}$ and $\mathfrak{n}$ would give the same result, with the arguments in the (symmetric) function ϕ exchanged.

For the Polyakov loop, we must compute the *difference* of the energy density with and without the background field,

$$e[\mathsf{a}] - e[0] = \int \frac{d^3p}{(2\pi)^3} \sum_{\mathfrak{m}=-\infty}^{\infty} e^{i\mathfrak{m}\beta p_z} \sum_{\sigma=\pm 1} [e^{i\mathfrak{m}\beta\sigma\mathsf{a}} - 1] \cdot g(\boldsymbol{p},\beta).$$

(132)

The term with $\mathfrak{m} = 0$ does not contribute and can be omitted. Furthermore, we can extend the σ sum to all roots $\sigma \in \{-1, 0, 1\}$, since the term with $\sigma = 0$ vanishes identically. This allows us to write the final result in the same form as the 1-loop contributions in Eq. (60),

$$e[\mathsf{a}] - e[0] = \sum_{\sigma} \sum_{\substack{\mathfrak{m} \in \mathbb{Z} \\ \mathfrak{m} \neq 0}} \int \frac{d^3p}{(2\pi)^3} e^{i\mathfrak{m}\beta p_z} [e^{i\mathfrak{m}\beta\sigma\mathsf{a}} - 1] \cdot g(\boldsymbol{p},\beta).$$

(133)

The main difference to the 1-loop term is that $g(\boldsymbol{p},\beta)$ from Eq. (131) is now itself a temperature-dependent loop integral instead of just a simple algebraic function. Except for the $\mathfrak{n} = 0$ term, all contributions to $g(\boldsymbol{p},\beta)$ only have a reduced $O(2)$ symmetry, i.e. they have an angular dependency which requires the use of Eq. (64) instead of Eq. (65) when evaluating Eq. (133). Combined with the sum over $\mathfrak{n}$ and the triple momentum integration, the numerical effort to compute the finite temperature corrections for the 2-loop contribution is easily three orders of magnitude larger than for the 1-loop case. Below, we will therefore use the same approximation as for the 1-loop contributions, where the $T = 0$ variation kernels and hence also the $T = 0$ limit of the functions $g(p)$ were used. This amounts to taking only the $\mathfrak{n} = 0$ contribution in Eq. (131), which is $O(3)$ symmetric and independent of temperature. In the numerics section, we will briefly justify this approximation *a posteriori*, i.e. we will show how to compute the first few $\mathfrak{n} \neq 0$ finite temperature corrections for selected momenta and assert that they are negligible as compared to the $T = 0$ term, even for temperatures up to $T = 2T^*$.

D. Renormalization of the 2-loop contribution

Our consideration on the Fourier transform in the last chapter indicate that Eq. (133) is finite provided that $g(\boldsymbol{p},\beta)$ does not rise stronger than $g(\boldsymbol{p},\beta) \sim |\boldsymbol{p}|$ at large momenta. This finiteness of the *outer* loop integration is due to the subtraction of the $\mathsf{a} = 0$ background in Eq. (133) and does not hold for other Green's functions. The possible divergences are thus all coerced in the *inner* loop integration in Eq. (131). The terms with $\mathfrak{n} \neq 0$ in that equation are finite as can be seen by the regulator method for the Fourier integral, or by appealing to Appendix C. This restricts possible divergences to the $T = 0$ contribution,

$$g_0(p) = \int \frac{d^3q}{(2\pi)^3} [2\phi(\boldsymbol{p},\boldsymbol{q}) + \phi(\boldsymbol{p},\boldsymbol{q}-\boldsymbol{p})].$$

(134)

The leading UV divergence is thus the contribution

$$g_0(p) = 3 \int \frac{d^3q}{(2\pi)^3} \phi(\boldsymbol{p},\boldsymbol{q}) + \cdots,$$

(135)

where the dots contain subleading divergences and finite pieces. To check this assertion, we can go back to the original expression (125) and use the results of Appendix C, where it was argued that only those terms in Eq. (125) are possibly divergent in which one of the two Poisson indices vanishes. Picking only these contributions and using the symmetry of $\phi(\boldsymbol{p},\boldsymbol{q})$, we find the leading divergence with a different prefactor[10]:

$$g_0(p) = 4 \int \frac{d^3q}{(2\pi)^3} \phi(\boldsymbol{p},\boldsymbol{q}) + \cdots.$$

(136)

The catch is that we had to shift the summation index and the loop momentum in divergent expression in order to derive Eq. (135). Such operations are known to change the UV divergence, which depends on the regularization scheme and the momentum and Poisson routing. The ambiguity must eventually be removed as part of the renormalization procedure. At present, we do not have a fully consistent method to renormalize our 2-loop contributions, by relating the necessary counterterms to physical observables. Instead, we take a pragmatic approach and *cancel* the divergences in whatever momentum routing is numerically convenient.[11]

Next we read off the core function $\phi(\boldsymbol{p},\boldsymbol{q})$ by comparing the general form Eq. (125) with the bosonic 2-loop contributions, Eqs. (108) and (122):

$$\phi(\boldsymbol{p},\boldsymbol{q}) = \frac{g^2}{16} \frac{3 - (\hat{\boldsymbol{p}} \cdot \hat{\boldsymbol{q}})}{\omega(\boldsymbol{p})\omega(\boldsymbol{q})} + \frac{[1 + (\hat{\boldsymbol{p}} \cdot \hat{\boldsymbol{q}})^2]}{16}$$

$$\cdot \frac{[\Omega(\boldsymbol{p}) - \Omega(\boldsymbol{q})]^2}{\omega(\boldsymbol{p})\omega(\boldsymbol{q})} \cdot V_C(\boldsymbol{p}+\boldsymbol{q}),$$

(137)

where $\Omega(\boldsymbol{p}) = \omega(\boldsymbol{p}) - \chi(\boldsymbol{p})$. With the $T = 0$ kernels, this depends on the momenta only in the combination $p = |\boldsymbol{p}|$, $q = |\boldsymbol{q}|$ and $\xi = \hat{\boldsymbol{p}} \cdot \hat{\boldsymbol{q}}$, i.e. we can write

$$\phi(\boldsymbol{p},\boldsymbol{q}) \equiv \Phi(p,q,\xi) = \frac{g^2}{16} \frac{3 - \xi}{\omega(p)\omega(q)} + \frac{1 + \xi^2}{16}$$

$$\cdot \frac{[\Omega(p) - \Omega(q)]^2}{\omega(p)\omega(q)} \cdot \frac{8\pi\sigma_C}{[p^2 + q^2 + 2\xi pq]^2}.$$

(138)

---

[10]One prefactor of 2 comes from setting $\mathfrak{m}$ or $\mathfrak{n}$ to zero, while the other factor of two comes from the color trace.

[11]We use Eq. (131) due to its close analogy to the 1-loop expressions.

The same dependency holds for the second term $\phi(\boldsymbol{p}, \boldsymbol{q} - \boldsymbol{p}) \equiv \Phi(p, Q, \eta)$ in the square bracket in Eq. (134), where

$$Q = |\boldsymbol{q} - \boldsymbol{p}| = \sqrt{p^2 + q^2 - 2\xi pq},$$

$$\eta = \cos \sphericalangle(\boldsymbol{p}, \boldsymbol{p} - \boldsymbol{q}) = \frac{q\xi - p}{Q}. \qquad (139)$$

As a consequence, the zero-temperature 2-loop contribution is $O(3)$ invariant, $g_0(\boldsymbol{p}) = g_0(p)$.

To find the possible UV divergences explicitly, take the Gribov form Eq. (91) for the gluon propagator $\omega(\boldsymbol{p})$ and Eq. (92) for the curvature $\chi(\boldsymbol{p})$ to, respectively, insert in Eqs. (137) and (134), and expand the integrand for large loop momenta. With a sharp momentum cutoff Λ, we obtain

$$g_0(p) = \frac{9g^2}{64\pi^2} \cdot \frac{\Lambda^2}{\omega(p)} + \frac{g^2\Lambda}{96\pi^2} \cdot \frac{p}{\omega(p)}$$
$$+ \frac{\sigma_C}{\pi} \ln\left(\frac{\Lambda}{\mu_0}\right) \cdot \frac{1}{\omega(p)} + \text{finite}, \qquad (140)$$

where μ_0 is an arbitrary scale parametrizing the finite piece in the log divergence. This function would then enter Eq. (65) for the Fourier transform, and eventually Eq. (68) to compute the effective potential for the Polyakov loop.

The linear divergence in Eq. (140) is absent if we either take a gauge-invariant regularization scheme, or consider the free case $\omega(k) = k$. In general, divergences and counterterms should not depend on the specific form of the variational solution.[12] We thus conclude that the linear divergence is spurious and should be canceled completely, if a hard momentum cutoff is used.

The remaining quadratic and logarithmic divergences are universal, i.e. they do not depend on the form of the variation kernels and persist even in the free case, $\omega(q) = q$. Their momentum dependence is identical and leads to a Fourier transform $h(\lambda)$ which vanishes at $\lambda = 0$, but goes to a nontrivial constant at $\lambda \to \infty$, cf. Fig. 8. As explained in the previous chapter, $h(0)$ counts the number of perturbative degrees of freedom, i.e. $h(0) = 0$ means that the Stefan-Boltzmann limit of the 1-loop calculation is preserved. Furthermore, the 1-loop bosonic contributions had $h_B(\infty) = 0$ leading to a very delicate confinement that is easily overcome by fermions. A nontrivial limit $h(\infty) \neq 0$ at small temperatures could thus be very helpful.

_____

[12]Furthermore, the momentum dependence $p/\omega(p)$ of the linear divergence is such that the corresponding Fourier transform $h(\lambda)$ vanishes both at $\lambda = 0$ and $\lambda \to \infty$, as can be seen from the left panel of Fig. 8. Even if present, it would therefore affect neither the Stefan-Boltzmann law at large temperatures nor confinement at small temperatures.

The counterterms for the inner loop integration would remove the divergence but leave a finite piece [see Eq. (140)],

$$\left[\frac{9g^2}{64\pi^2} \cdot \Lambda^2 + \frac{\sigma_C}{\pi} \ln\left(\frac{\Lambda}{\mu_0}\right)\right] \cdot \frac{1}{\omega(p)} \to c_2 \cdot \frac{\sigma_C}{\omega(p)}. \qquad (141)$$

As explained earlier in the 1-loop case, the dimensionless coefficient c_2 should be fixed by relating it to another physical input observable or fitting to lattice data. Renormalization would then remove the divergence and trade the coupling g for the (dimensionfull) input quantity or the scale in the lattice data. This is beyond the scope of the present paper. Instead, we take the same pragmatic approach as in the 1-loop case and treat c_2 and g as free parameters. This allows us to study e.g. how different values of c_2 could affect the physical outcome.

With these arrangements, the renormalized inner loop integral (131) becomes (using a sharp momentum cutoff),

$$g_0(p) = \frac{1}{4\pi^2} \int_0^\infty dq \left[q^2 \int_{-1}^1 d\xi (2\Phi(p, q, \xi)\right.$$
$$\left. + \Phi(p, Q, \eta)) - \Phi_\infty(p, q)\right] + c_2 \frac{\sigma_C}{\omega(p)}, \qquad (142)$$

with the subtraction

$$\Phi_\infty(p, q) = \left[\frac{9g^2}{8} q + \frac{g^2}{24} p + \frac{4\pi\sigma_C}{q} \tanh(q/\sqrt{\sigma_C})\right] \frac{1}{\omega(p)}. \qquad (143)$$

The tanh is introduced to avoid the infrared singularity arising from the subtraction of the logarithmic UV divergence. This could be replaced by any other regulator function $f(q)$ with the limits $f(\infty) = 1$ and $f(q) \sim q$ at $q \to 0$. A different regulator $f(q)$ would amount to a slightly different subtraction of the form of a finite numerical constant times $1/\omega(p)$. This can always be absorbed by a slight change of the renormalization parameter c_2.

E. Numerical results

1. Core function at zero temperature

For our numerical code, we measure all dimensionfull quantities in units of the Coulomb string tension, i.e. we use the mass scale $\sqrt{\sigma_C}$ from here on. First, we compute the inner loop integration (core function) $g_0(p)$ from Eq. (142). In the left panel of Fig. 9, we show $g_0(p)$ for $c_2 = 0$ and various values of the coupling $\alpha = g^2/(4\pi)$. To put this in perspective, we have also included the 1-loop contribution $g_B(p) = \omega(p) - \chi(p)$. From the plot, it is clear that the 2-loop corrections are small in magnitude (even at couplings of order unity) for most momenta, but they dominate
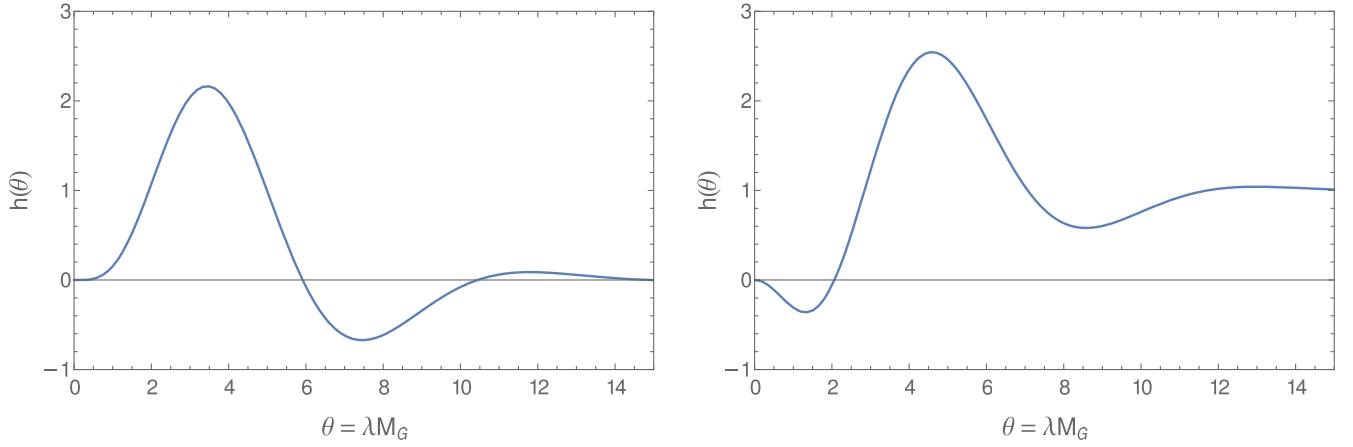
FIG. 8.   The Fourier transform $h(\lambda)$ from Eq. (65) for the momentum dependencies $g(p)$ encountered in 2-loop divergences. Left: $g(p) \sim p/\omega(p)$ (spurious linear divergence). Right: $g(p) \sim 1/\omega(p)$ (quadratic and log divergence).
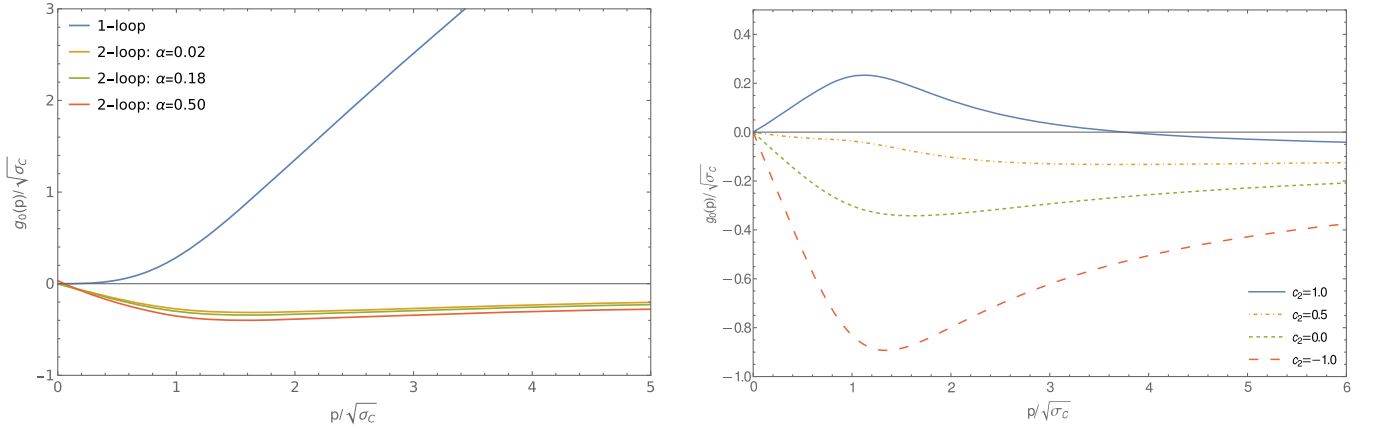

FIG. 9.   Left: the inner loop integral (core function) $g_0(p)$ for the renormalization parameter $c_2 = 0$ at various couplings $\alpha = g^2/4\pi$. Right: the core function at the preferred coupling $\alpha = 0.18$ for various values of c_2.

at small momenta because of the cancellation in the 1-loop result mentioned earlier. This will help to make the bosonic confinement more robust.

We have varied the coupling α in the expected region by a factor of 25 and found only a mild effect on the 2-loop result. Furthermore, the parameters g and c_2 are related, i.e. changes in g can largely be compensated by changes in c_2. In the following, we will therefore fix g to a reasonable value $g = 1.5$ corresponding to $\alpha = g^2/4\pi = 0.18$ and vary only c_2.

In the right panel of Fig. 9, we plot $g_0(p)$ at the preferred g and various values of c_2. Negative values increase the confining effect by making $g_0(p)$ more negative at small momenta. By contrast, positive values have the opposite effect and may reduce (or even destroy) the confining property. Note that we also expect that a strong confinement leads to a higher transition temperature, as more thermal fluctuations are necessary to overcome the confining order.

2. Finite temperature corrections

Next, we want to corroborate that the finite temperature corrections to $g_0(p)$ are indeed negligible. We take the $\mathfrak{n} \neq 0$ terms from Eq. (131) and combine the mirror pairs $\pm\mathfrak{n}$. Then we introduce spherical coordinates and consider each Poisson index $\mathfrak{n} \geq 1$ separately. Since we no longer have $O(3)$ symmetry, the external momentum $\boldsymbol{p}$ cannot be rotated to the z direction, but only to the xy plane. As usual, we replace the polar and azimuthal angles by their cosine, $\xi_p = \cos\vartheta_q$ or $\gamma_q = \cos\varphi_q$ etc. The finite temperature corrections to $g_0(p)$ then read

$$g_{\mathfrak{n}}(\boldsymbol{p},\beta) = g_{\mathfrak{n}}(p,\xi_p,\beta)$$

$$= \frac{1}{\pi^3} \int_0^\infty dq\, q^2 \int_{-1}^1 d\xi_q \int_{-1}^{+1} \frac{d\gamma_q}{\sqrt{1-\gamma_q^2}}$$

$$\times \cos(\mathfrak{n}\beta q\xi_q)[2\phi(\boldsymbol{p},\boldsymbol{q}) + \phi(\boldsymbol{p},\boldsymbol{q}-\boldsymbol{p})]. \quad (144)$$
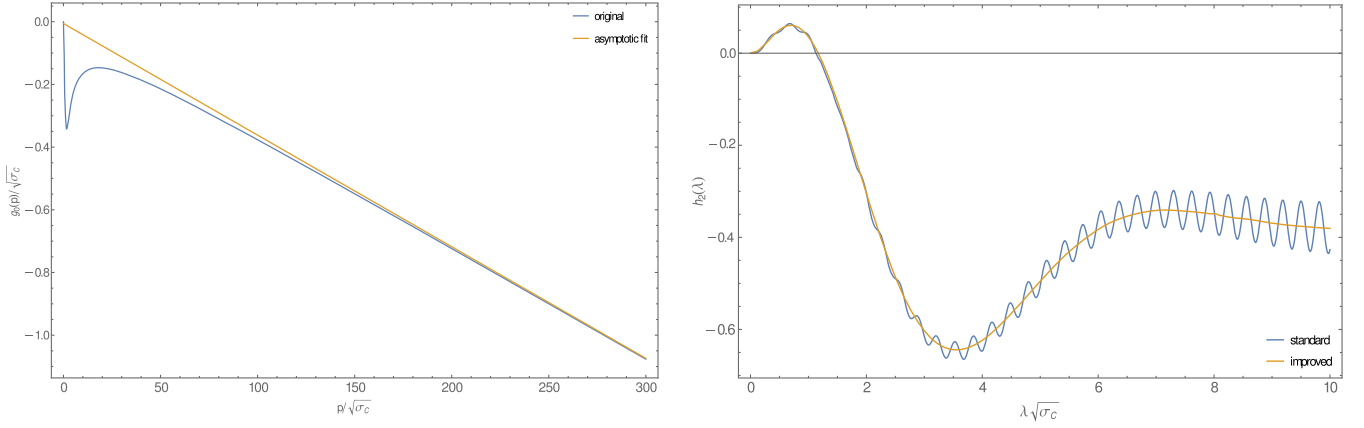
FIG. 10. Left: the 2-loop core function $g_0(p)$ with its asymptotics at large momenta $p \gg 1$. Right: the 2-loop Fourier transform $h_2(\lambda)$ computed with and without the improved regularization technique Eq. (146).

Since this is not $O(3)$ symmetric, we also have to average over the angle ξ_p using Eq. (66). The parameter in that average is $\lambda = \mathfrak{m}\beta$. Larger values of $\mathfrak{m} \geq 1$ are strongly suppressed by the factor $1/m^4$ in the effective action of the Polyakov loop Eq. (68), and we expect the largest finite temperature corrections from $\mathfrak{m} = 1$, i.e. $\lambda = \beta$. In total,

$$g_{\mathfrak{n}}(p, \beta) \simeq \frac{1}{2\pi^3} \frac{\beta p}{\sin(\beta p)} \int_0^\infty dq \, q^2 \int_{-1}^1 d\xi_p \int_{-1}^1 d\xi_q$$
$$\times \int_{-1}^1 \frac{d\gamma_q}{\sqrt{1 - \gamma_q^2}} \cos(\beta p \xi_p) \cos(\mathfrak{n}\beta q \xi_q)$$
$$\times [2\Phi(p, q, \xi) + \Phi(p, Q, \eta)]. \tag{145}$$

In this equation, Q and η are defined as in Eq. (139), with the angle ξ now computed from

$$\xi \equiv \hat{\boldsymbol{p}} \cdot \hat{\boldsymbol{q}} = \xi_p \xi_q + \gamma \sqrt{(1 - \xi_p^2)(1 - \xi_q)^2}.$$

As can be expected, the fourfold integral (145) is numerically quite challenging, although the three angular integrations can usually be done efficiently using Gauss-Legendre techniques. We have computed the correction Eq. (145) for $\mathfrak{n} \leq 5$, spot values of the momentum and selected temperatures between 100 and 450 MeV, and found that the result is generally of the order or even smaller than the numerical accuracy in $g_0(p)$. This confirms that we can make the same approximation as in the 1-loop case, viz. replace the core function entering the calculation of the Polyakov loop by its $T \to 0$ limit.

3. Fourier transform of the 2-loop contribution

The next step is to Fourier transform the core function $g_0(p)$ according to Eq. (65), which yields the temperature-dependent 2-loop amplitude $h_2(\lambda = \mathfrak{m}\beta)$. The regulator method shows numerical instabilities (oscillations) that

worsen at large λ, cf. Fig. 10. The cause of the problem can be traced to the fact that our 2-loop core function $g_0(p)$ does not vanish at large momenta, which makes the computation of the Fourier transform rather delicate. Since we cannot compute $g_0(p)$ for arbitrarily large p, we would have to cut off the Fourier integral at some upper limit Λ. This leads to typical oscillations of the type

$$g_0(\Lambda) \frac{\lambda\Lambda\cos(\lambda\Lambda) - \sin(\lambda\Lambda)}{\lambda^2}.$$

The point here is that we must not introduce boundary terms by a hard cutoff to the Fourier integral, since boundaries at large but finite momenta spoil the regulator method. Numerically, $g_0(p)$ actually becomes *linear* at large momenta, albeit with a very small slope, cf. the left panel of Fig. 10. We determine the coefficients a and b from a linear regression $g_0(p) \simeq a + bp$ at large $p \geq \Lambda \simeq 200$ and find the small values $a = -0.0057$ and $b = -0.00356$. After subtracting the asymptotics, the Fourier integration can be done, and the subtracted linear function can be transformed analytically[13] and added back in:

$$-\frac{\lambda^3}{2} \lim_{\mu \to 0} \int_0^\infty dp \, p \sin(\lambda p) e^{-\mu p} [g_0(p) - (a + b \cdot p)] + b. \tag{146}$$

The result of this procedure is a much smoother Fourier integration without the numerical artifacts, cf. again the right panel of Fig. 10.

In the next Fig. 11 we first present the results of the regulator method. The Fourier transform converges nicely when $\mu \to 0$, but it requires quite small values to reach the

---

[13]According to Eq. (89), the regulator method gives $\lim_{\mu \to 0} \frac{-\lambda^3}{2} \int_0^\infty dp \, p \sin(\lambda p) e^{-\mu p}(a + bp) = b$.
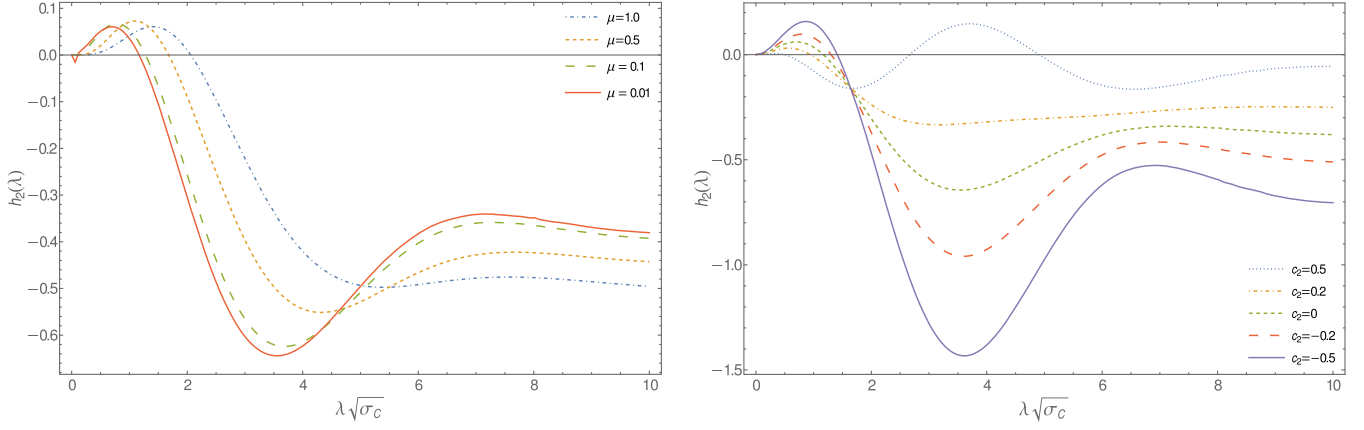
FIG. 11. Left: the approach to the limiting function $h_2(\lambda)$ as the regulator is removed. Right: the 2-loop Fourier amplitude $h_2(\lambda)$ computed for several values of the renormalization parameter c_2.

limit. In practice, we have decreased μ progressively in up to 20 steps and used Richardson extrapolation to the limit $\mu \to 0$.

The right panel of Fig. 11 shows the Fourier amplitude $h_2(\lambda)$ for the preferred coupling $\alpha = 0.18$ and several values of the renormalization constant c_2. All functions $h_2(\lambda)$ vanish at the origin, which means that the mode count at high temperatures and the Stefan-Boltzmann law from 1-loop is preserved. Negative values for c_2 increase the negative constant $h_2(\infty)$ and hence the strength of the bosonic confinement, while also increasing the deconfinement temperature. Conversely, positive values for c_2 have the opposite effect of weakening or even destroying confinement if taken too large. However, such large values of $|c_2|$ overemphasize the 2-loop contribution, which should remain a subleading effect. Coefficients $|c_2| \le 0.2$ are natural and seem to exhibit the correct qualitative behavior.

4. The Polyakov loop

Let us now collect all the pieces and study the effect of the 2-loop corrections on the Polyakov loop. Figure 12 shows our cumulative results for the expectation value of the Polyakov loop as a function of temperature. The renormalization constant for the 1-loop terms is fixed to the preferred value $c_0 = 0$, and the 2-loop contribution is varied in the range $c_2 \in [0, -1.0]$ as discussed earlier.

In the left panel, we show only the gluon contribution at 1- and 2-loop levels. As expected, the inclusion of the 2-loop terms make for a stronger gluon confinement, so that the critical temperature rises. The effect is not dramatic, as critical temperatures of $T^* \approx 300$ MeV are still in agreement with lattice calculations, in particular since the Coulomb string tension determining the absolute scale is not known to high precision. The onset of confinement when cooling the system seems to be somewhat softer at
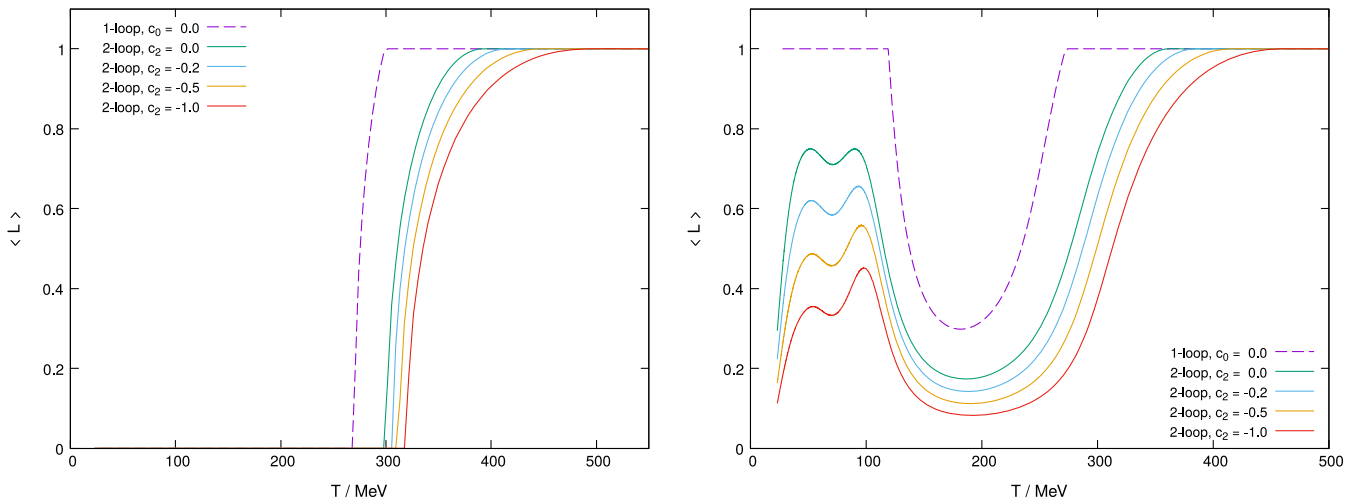

FIG. 12. The Polyakov loop as a function of temperature for various values of the 2-loop renormalization constant c_2. For reference, the 1-loop findings is also included. The left panel shows the pure Yang-Mills case, while the right panel includes $N_f = 2$ flavors of (light) quarks. All plots are made with the preferred value $c_0 = 0$ for the mass counterterm.
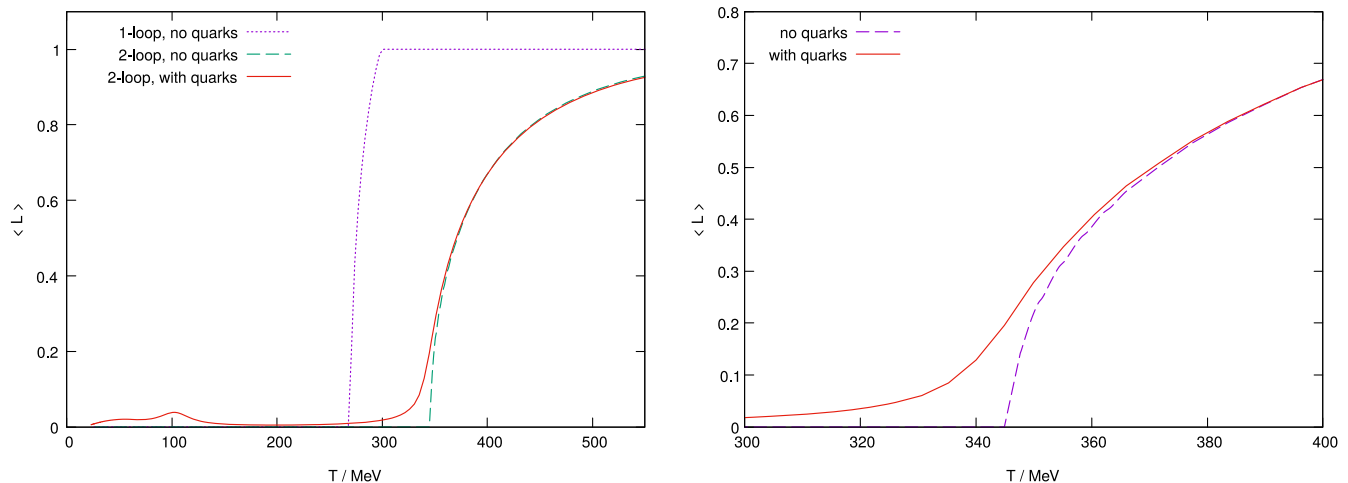
FIG. 13.   The Polyakov loop for an extreme value of the renormalization parameter $c_2 = -20$, which (over)emphasizes the 2-loop contribution. The left panel shows the entire temperature range, while the right panel highlights the region near the phase transition.

2-loop order, but the overall qualitative features and the order of the phase transition remain unchanged.

After including quarks, the picture changes qualitatively, as can be seen from the right panel of Fig. 12. We haven taken $N_f = 2$ flavors and included the 1-loop result for reference. At 1-loop level, the confinement is incomplete and reverts to a fully deconfined phase as we cool the system below $T \simeq 100$ MeV. As we switch on the 2-loop contribution, this unphysical phase becomes suppressed by the stronger gluon confinement, although the original tendency to increase the Polyakov loop in this region remains clearly visible. We could say that the unphysical deconfined phase is replaced by a region of *incomplete* confinement, with the separation energy for two static color sources being large, but not infinite. At *very* low temperatures, the Polyakov loop always vanishes $\langle L \rangle = 0$, irrespective of the renormalization parameter. This is different from the 1-loop results, where the unphysical phase seems to persists up to $T = 0$.

As we have mentioned above, larger values of $-c_2$ tend to strengthen the gluon confinement by emphasizing the bosonic 2-loop contribution. At the same time, this also increases the (pseudo)critical temperature as more thermal fluctuations are necessary to overcome the confining order. For curiosity, we have explored the extreme case of $c_2 = -20$ in Fig. 13. The unphysical effects in the confined phase are now completely suppressed except for a tiny bump near $T = 100$ MeV. At the same time, the critical temperature in the Yang-Mills case increases to about $T^* = 344$ MeV due to the strong gluon confinement.

In the right panel of Fig. 13, we highlight the temperature region near the phase transition. It is clearly seen that the quarks have the tendency to weaken the transition, which changes from a strong second order transition in the pure Yang-Mills case to a *crossover*. The pseudocritical temperature for this crossover is, however, not lowered

substantially compared to the pure Yang-Mills T^*. The quarks have practically no effect in the deconfined region as well, and only affect the physics close to the phase transition.

VI. SUMMARY AND CONCLUSION

In this paper, we have studied the Polyakov loop and the deconfinement phase transition within the Hamiltonian approach to QCD. We found excellent agreement with lattice data for the pure Yang-Mills case, but an unphysical deconfined phase at low temperatures as we introduce one or two flavors of light quarks. This phenomenon could be traced to the weakness of the gluon confinement in the Hamiltonian approach, since the effective potential for the Polyakov loop becomes very small at low temperatures and the center symmetric phase is thus only slightly lower (in free energy) than its center-broken counterpart. Even $N_f = 1$ flavor of light quarks can thus easily overcome the bosonic order and deconfine the system at low temperatures.

Since the shortcoming of the Hamiltonian approach at 1-loop level is clearly in the gluon sector, we have studied the effect of including the neglected 2-loop gluon contributions. (The quark 2-loop terms will not make a qualitative difference.) As in the 1-loop case, we treat the renormalization constant c_2 arising at this order as a free parameter, which can be tuned to control the strength of the 2-loop effects. Though the numerical effort is several orders of magnitude larger, we were able to compute the 2-loop corrections with high accuracy and study a wide range of parameters. We find that the 2-loop terms indeed strengthen the gluon confinement and partially suppress the unphysical effects in the confined phase. This suppression becomes stronger as we increase the renormalization constant c_2 to emphasize the 2-loop terms. At the same

time, the stronger confinement increases the critical temperature in the Yang-Mills case to about $T^* \approx 300$ MeV, which is still supported by lattice results.

To completely suppress the unphysical effects in the confined phase, we had to take the 2-loop renormalization parameter to rather extreme values $c_2 \approx -20$. This is a rather unnatural setup, because the 2-loop terms start to dominate and it general remains unclear how such a large value for $|c_2|$ should emerge naturally. Nonetheless, it is interesting to see that the quarks in this scenario affect only the region near the transition, turning the second order transition to a crossover. The (pseudo)critical temperature in the extreme scenario rises to about 344 MeV.

There are several ways in which our findings could be further improved. First, a full renormalization should be carried out that fixes the constants c_0 and c_2 at 1- and 2-loops level by relating it to a physical input quantity. This should, in particular, clarify if large values of c_2 as in the previous scenario are physically sensible. Furthermore, we could include the fermion 2-loop terms to have a complete description at 2 loops, as well as the finite temperature corrections to the kernels and core functions. We do not expect these terms to contribute significantly, while the computational effort would increase considerably. A better strategy might be to incorporate the effects of higher loops and finite temperature in the gluon variational kernels already at 1-loop. This might require to deviate substantially from the Gaussian *Ansatz*, which we plan to investigate in a future study.

APPENDIX A: ROOT DECOMPOSITION OF $SU(N)$

The semisimple Lie algebra $SU(N)$ has rank $r = (N-1)$ and there are hence r mutually commuting generators H_k which span the Cartan subalgebra of $SU(N)$. As explained in the main text, the background field a must be chosen in the Cartan subalgebra,

$$\mathsf{a} = \sum_{k=1}^{r} \mathsf{a}^k H_k.$$

Since the H_k are anti-Hermitian and mutually commuting, they can be simultaneously diagonalized with purely imaginary eigenvalues $(-i\mu_k)$. The real numbers μ_k are called the weights of H_k, and the collection of one eigenvalue from each H_k forms a weight vector $\underline{\mu} = (\mu_1, ..., \mu_r)$. The number of such vectors, i.e. the number of the eigenvalues of H_k depends on the representation. In the fundamental representation, for instance, H_k is $(N \times N)$ and there are hence N weight vectors.

In the present paper, we are mainly concerned with the background field in the *adjoint* representation, $\hat{\mathsf{a}}^{ab} = -f^{abc}\mathsf{a}^c$. The weights σ_k in the adjoint representation are called the roots,

$$\hat{H}_k|\sigma\rangle = -i\sigma_k|\sigma\rangle, \tag{A1}$$

and the real numbers σ_k from all Cartan generators are collected in root vectors $\underline{\sigma} = (\sigma_1, ..., \sigma_r)$. The corresponding eigenvector $|\sigma\rangle$ diagonalizes all generators $\hat{H}_k$ simultaneously. Since $\hat{H}_k$ is $(N^2 - 1) \times (N^2 - 1)$ dimensional, the eigenvector $|\sigma\rangle$ is an adjoint color vector with $N^2 - 1$ components $\angle a|\sigma\rangle$, and there can be at most $(N^2 - 1)$ such eigenvectors and hence $(N^2 - 1)$ root vectors. Of these roots, $r = (N - 1)$ must vanish and the entire root system of $SU(N)$ thus contains $N(N-1)$ nonvanishing root vectors. They can be given a partial ordering by the first element, i.e. the eigenvalues of $\hat{H}_1$. Then the nonvanishing roots $\underline{\sigma}$ come in pairs $\pm\sigma$ and half of them are positive, half of them are negative. From Eq. (A1), the adjoint background field is diagonal in the basis $|\sigma\rangle$,

$$\hat{\mathsf{a}}|\sigma\rangle = -i(\mathsf{a} \cdot \underline{\sigma})|\sigma\rangle = -i\left(\sum_{k=1}^{r} \mathsf{a}_k \sigma_k\right)|\sigma\rangle.$$

The color group $G = SU(2)$ has rank $r = 1$ and both the root and weight vectors are pure numbers. There are two weights $\pm\frac{1}{2}$ and three roots $\{-1, 0, 1\}$, of which only two are nonvanishing. The corresponding eigenvectors in the adjoint are the well-known cyclic basis,

$$|\sigma = 1\rangle = -\frac{1}{\sqrt{2}}\begin{pmatrix} 1 \\ i \\ 0 \end{pmatrix}, \qquad |\sigma = 0\rangle = \begin{pmatrix} 0 \\ 0 \\ 1 \end{pmatrix},$$

$$|\sigma = -1\rangle = \frac{1}{\sqrt{2}}\begin{pmatrix} 1 \\ -i \\ 0 \end{pmatrix}.$$

This structure easily generalizes to $G = SU(3)$, which has rank $r = 2$. The two Cartan generators are usually taken as $H_1 = T_3 = \lambda_3/(2i)$ and $H_2 = T_8 = \lambda_8/(2i)$ in terms of Gell-Mann matrices. The root and weight vectors are both two dimensional. Explicitly, the weights read

$$\underline{\mu}: \left(0, \frac{1}{\sqrt{3}}\right), \qquad \left(\frac{1}{2}, \frac{1}{2\sqrt{3}}\right), \qquad \left(\frac{1}{2}, -\frac{1}{2\sqrt{3}}\right).$$

More important are the $N^2 - 1 = 8$ root vectors, of which $N(N-1) = 6$ are nonvanishing. As they come in pairs with opposite sign of σ_1, there are three nonvanishing positive roots

$$\underline{\sigma}: (1, 0), \qquad \left(\frac{1}{2}, \frac{1}{2}\sqrt{3}\right), \qquad \left(\frac{1}{2}, -\frac{1}{2}\sqrt{3}\right). \tag{A2}$$

From these roots, it is clear that any $SU(3)$ background field in the Cartan algebra, $\mathsf{a} = \mathsf{a}^3 T^3 + \mathsf{a}^8 T^8$ can conveniently be described by the rescaled components

$$x = \frac{\beta a^3}{2\pi}, \qquad y = \frac{\beta a^8}{2\pi}. \tag{A3}$$

The fundamental domain (Weyl alcove) in these variables is triangular; if complemented by two half-alcoves, it is given by the rectangle

$$x \in [0, 1], \qquad y \in \left[0, \frac{2}{\sqrt{3}}\right]. \tag{A4}$$

Finally, the momentum shift p_σ for the three positive roots is

$$\underline{\sigma} = (0, 1): \qquad p_\sigma = \frac{2\pi}{\beta} x,$$

$$\underline{\sigma} = \left(\frac{1}{2}, \frac{1}{2}\sqrt{3}\right): \qquad p_\sigma = \frac{\pi}{\beta}(x + \sqrt{3}y),$$

$$\underline{\sigma} = \left(\frac{1}{2}, -\frac{1}{2}\sqrt{3}\right): \qquad p_\sigma = \frac{\pi}{\beta}(x - \sqrt{3}y). \tag{A5}$$

The structure constants f^{abc} of the $su(N)$ algebra can also be transformed to the Cartan basis,

$$f_{\rho,\sigma,\tau} = f^{abc}\langle a|\rho\rangle\langle b|\sigma\rangle\langle c|\tau\rangle.$$

They are still antisymmetric, and most relations for the original structure constants have simple counterparts in the Cartan basis. For instance, from $f^{abc}f^{a'bc} = N\delta^{aa'}$ (sum over repeated indices) we have

$$\sum_{\rho,\sigma,\tau} |f_{\rho,\sigma,\tau}|^2 u(\underline{\rho}\cdot\underline{a}) = N\sum_\rho u(\underline{\rho}\cdot\underline{a}),$$

$$\sum_{a,b,c} |f^{abc}|^2 = \sum_{\rho,\sigma,\tau} |f_{\rho,\sigma,\tau}|^2 = N(N^2 - 1). \tag{A6}$$

APPENDIX B: SELF-CONSISTENT 2-LOOP ENERGY

In the main text, it has been stressed repeatedly that the gap equation mixes loop orders, and the self-consistent 1-loop energy already contains parts of the 2-loop terms. This raises the question whether the self-consistent 2-loop energy must be corrected to avoid double counting.

To clarify this point, it is sufficient to work at $T = 0$ without a background field; the modifications for the general case are straightforward. We write the complete energy in the gluon sector (39) in the form

$$E_B = \langle H_B \rangle = \frac{1}{2}V_3(N^2 - 1)\int \frac{d^3q}{(2\pi)^3}\frac{\Omega(q)^2 + q^2}{\omega(q)} + E_2, \tag{B1}$$

where $\Omega(q) \equiv \omega(q) - \chi(q)$, and E_2 denotes all 2-loop contributions. Note that this expression is valid for *any* kernel $\omega(q)$, irrespective of whether it satisfies the gap equation or not. To minimize the energy, we now take the variation with respect to the propagator $\omega(k)^{-1}$, set it to zero and cancel the common factor

$$c \equiv \frac{2(2\pi)^3}{V_3(N^2 - 1)}. \tag{B2}$$

Further evaluation, using $\delta\omega(q)/\delta\omega^{-1}(k) = -\omega(q)^2\delta(q-k)$ yields the gap equation in the form

$$\omega(k)^2 = k^2 + \chi(k)^2 - 2\nu(k) + c\frac{\delta E_2}{\delta\omega^{-1}(k)}. \tag{B3}$$

Here, we have obtained an additional 2-loop contribution through the implicit dependency of the curvature on the gluon kernel,

$$\nu(k) \equiv \int d^3q \frac{\Omega(q)}{\omega(q)}\frac{\delta\chi(q)}{\delta\omega^{-1}(k)}.$$

This term is usually neglected in the gap equation, and we will also do so in the present paper. For the moment, however, we keep this term and insert the gap equation back into the full energy Eq. (B1) to obtain the total self-consistent energy. After a straightforward calculation,

$$E_B^{\text{sc}} = V_3(N^2 - 1)\int \frac{d^3q}{(2\pi)^3}[\Omega(q) + \epsilon(q)] + E_2^{\text{sc}}, \tag{B4}$$

where the (self-consistent) 2-loop contributions read explicitly

$$\epsilon(q) = \int d^3p \frac{\Omega(p)}{\omega(p)}\omega(q)^{-1}\frac{\delta\chi(p)}{\delta\omega^{-1}(q)}, \tag{B5}$$

$$E_2^{\text{sc}} = E_2 - \int d^3q\, \omega(q)^{-1}\frac{\delta E_2}{\delta\omega^{-1}(q)}. \tag{B6}$$

These formulas for the total boson energy are only valid for solutions of the gap equation (B3). If we follow the standard approach and neglect the implicit dependency of the curvature on the gluon kernel, $\epsilon(q) \approx 0$, it becomes evident that the first term in Eq. (B4) is precisely the self-consistent 1-loop energy, which was used back in Eq. (50) in the main text. The second term, E_2^{sc}, is therefore the *self-consistent 2-loop energy*. As can be seen from Eq. (B6), E_2^{sc} *differs* from the original 2-loop term E_2 by a subtraction—this is precisely the subtraction necessary to compensates for the 2-loop terms which have been moved into the self-consistent 1-loop contribution via the gap equation.

The subtraction in E_2^{sc} can be substantial: if the functional E_2 is e.g. quadratic in the propagator $\omega(k)^{-1}$, then it

is easily seen that $E_2^{sc} = -E_2$, i.e. the 2-loop contribution flips the sign. Fortunately, only the $T = 0$ tadpole contribution from the non-Abelian magnetic field is affected by this subtlety, and this term drops out when computing the Polyakov loop.

APPENDIX C: FINITENESS OF THE NON-ABELIAN MAGNETIC CONTRIBUTION

In the following, we show that all contributions to the non-Abelian magnetic energy, Eq. (108), with both Poisson indices nonvanishing, are UV *finite*—provided that the same regularization procedure for the momentum integrals as in the 1-loop terms is employed, cf. Eq. (89). For the proof it is sufficient to consider the most singular terms in Eq. (108) only, i.e. we can ignore the angular dependency $(\hat{p} \cdot \hat{q})$ in the numerator against the constant 3 and, furthermore, replace the full gluon energy $\omega(p)$ by its perturbative form p. Then the terms of Eq. (108) with no zero Poisson indices $\mathfrak{m} \neq 0 \neq \mathfrak{n}$ become

$$\langle \widetilde{H_{YM}^{NA}} \rangle_0 = \frac{3g^2}{16} V_2 \beta \frac{1}{(2\pi)^4} \int_0^\infty dp\, p \int_0^\infty dq\, q \sum_{\rho,\sigma,\tau} |f_{\rho,\sigma,\tau}|^2$$

$$\times \sum_{\substack{\mathfrak{m}=-\infty \\ \mathfrak{m} \neq 0}}^\infty \int_{-1}^1 dz\, e^{i\mathfrak{m}\beta(pz+\underline{\sigma}\cdot\underline{a})} \sum_{\substack{\mathfrak{n}=-\infty \\ \mathfrak{n} \neq 0}}^\infty \int_{-1}^1 dy\, e^{i\mathfrak{n}\beta(yq+\underline{\tau}\cdot\underline{a})}. \tag{C1}$$

Performing the z and y integrals gives

$$\langle \widetilde{H_{YM}^{NA}} \rangle_0 = \frac{3g^2}{(2\pi)^4} V_2 \beta \sum_{\rho,\sigma,\tau} |f_{\rho,\sigma,\tau}|^2 I(\underline{\sigma} \cdot \underline{a}) I(\underline{\tau} \cdot \underline{a}), \tag{C2}$$

where we have introduced the abbreviation

$$I(x) \equiv \int_0^\infty dp\, p \sum_{\mathfrak{m}=1}^\infty \frac{\sin(\mathfrak{m}\beta p)}{\mathfrak{m}\beta p} \cos(\mathfrak{m}\beta x). \tag{C3}$$

At this point, we can use Eq. (89) with $\alpha = -1$ to carry out the p integral,

$$I(x) = \sum_{\mathfrak{m}=1}^\infty \frac{\cos(\mathfrak{m}\beta x)}{(\mathfrak{m}\beta)^2} = \frac{1}{\beta^2} \left[\frac{\pi^2}{6} - \frac{\pi}{2}\beta x + \frac{1}{4}(\beta x)^2 \right],$$

$$x \in [0, 2\pi]. \tag{C4}$$

After inserting this result in Eq. (C2), we must carry out the remaining summation over the roots. Since we are only interested in the finiteness of the loop integrals, it is sufficient to consider the color group $G = SU(2)$, for which the $N^2 - 1 = 3$ roots are given by $\sigma \in \{0, \pm 1\}$ and

$$\sum_{\rho,\sigma,\tau} |f_{\rho,\sigma,\tau}|^2 I(\underline{\sigma} \cdot \underline{a}) I(\underline{\tau} \cdot \underline{a}) = 2I(a)^2 + 4I(a)I(0). \tag{C5}$$

Inserting finally Eq. (C5) into Eq. (C2) and subtracting the zero-background field contribution, we obtain eventually

$$\langle \widetilde{H_{YM}^{NA}} \rangle_0 - \langle \widetilde{H_{YM}^{NA}} \rangle_0 |_{a=0} = \frac{3g^2}{8\pi^4} \beta V_2 [I(a) - I(0)]$$

$$\cdot [I(a) + 3I(0)]. \tag{C6}$$

By Eq. (C4), this is indeed finite for all background fields a.

---

[1] F. Karsch, Lect. Notes Phys. **583**, 209 (2002).

[2] K. Fukushima and T. Hatsuda, Rep. Prog. Phys. **74**, 014001 (2011).

[3] C. Gattringer and K. Langfeld, Int. J. Mod. Phys. A **31**, 1643007 (2016).

[4] C. S. Fischer, J. Phys. G **32**, R253 (2006); R. Alkofer and L. von Smekal, Phys. Rep. **353**, 281 (2001); D. Binosi and J. Papavassiliou, Phys. Rep. **479**, 1 (2009); L. Fister and J. M. Pawlowski, Phys. Rev. D **88**, 045010 (2013).

[5] J. M. Pawlowski, Ann. Phys. (Amsterdam) **322**, 2831 (2007); F. Marhauser and J. M. Pawlowski, arXiv:0812 .1144; H. Gies, Lect. Notes Phys. **852**, 287 (2012); T. K. Herbst, J. Luecker, and J. M. Pawlowski, arXiv:1510 .03830.

[6] M. Quandt, H. Reinhardt, and J. Heffner, Phys. Rev. D **89**, 065037 (2014); M. Quandt and H. Reinhardt, Phys. Rev. D **92**, 025051 (2015).

[7] U. Reinosa, J. Serreau, M. Tissier, and N. Wschebor, Phys. Rev. D **93**, 105002 (2016).

[8] M. Peláez, U. Reinosa, J. Serreau, M. Tissier, and N. Wschebor, Rep. Prog. Phys. **84**, 124202 (2021); D. M. van Egmond, U. Reinosa, J. Serreau, and M. Tissier, SciPost Phys. **12**, 087 (2022); D. Dudal, D. M. van Egmond, U. Reinosa, and D. Vercauteren, Phys. Rev. D **106**, 054007 (2022).

[9] C. Feuchter and H. Reinhardt, Phys. Rev. D **70**, 105021 (2004); H. Reinhardt and C. Feuchter, Phys. Rev. D **71**, 105002 (2005); D. Epple, H. Reinhardt, and W. Schleifenbaum, Phys. Rev. D **75**, 045011 (2007); M. Pak and H. Reinhardt, Phys. Rev. D **88**, 125021 (2013); P. Vastag, H. Reinhardt, and D. Campagnari, Phys. Rev. D **93**, 065003 (2016).

[10] H. Reinhardt, G. Burgio, D. Campagnari, E. Ebadati, J. Heffner, M. Quandt, P. Vastag, and H. Vogt, Adv. High Energy Phys. **2018**, 1 (2018).

[11] M. Alford, K. Rajagopal, and F. Wilczek, Phys. Lett. B **422**, 247 (1998).

[12] M. G. Alford, A. Schmitt, K. Rajagopal, and T. Schäfer, Rev. Mod. Phys. **80**, 1455 (2008).

[13] B. Svetitsky, Phys. Rep. **132**, 1 (1986); R. V. Gavai, Nucl. Phys. **B215**, 458 (1983).

[14] B. Lucini, M. Teper, and U. Wenger, J. High Energy Phys. 02 (2005) 033.

[15] J. Braun, H. Gies, and J. M. Pawlowski, Phys. Lett. B **684**, 262 (2010).

[16] J. Braun and T. K. Herbst, arXiv:1205.0779.

[17] A. Bazavov, H.-T. Ding, P. Hegde, O. Kaczmarek, F. Karsch, N. Karthik, E. Laermann, A. Lahiri, R. Larsen, S.-T. Li, S. Mukherjee, H. Ohno, P. Petreczky, H. Sandmeyer, C. Schmidt, S. Sharma, and P. Steinbrecher, Phys. Lett. B **795**, 15 (2019).

[18] A. Dumitru, Y. Guo, Y. Hidaka, C. P. K. Altes, and R. D. Pisarski, Phys. Rev. D **86**, 105017 (2012).

[19] J. Heffner, H. Reinhardt, and D. R. Campagnari, Phys. Rev. D **85**, 125029 (2012).

[20] H. Reinhardt, Phys. Rev. D **94**, 045016 (2016).

[21] H. Reinhardt and J. Heffner, Phys. Lett. B **718**, 672 (2012).

[22] H. Reinhardt and J. Heffner, Phys. Rev. D **88**, 045024 (2013).

[23] J. Heffner and H. Reinhardt, Phys. Rev. D **91**, 085022 (2015).

[24] D. R. Campagnari, E. Ebadati, H. Reinhardt, and P. Vastag, Phys. Rev. D **94**, 074027 (2016).

[25] S. Adler and A. Davis, Nucl. Phys. **B244**, 469 (1984).

[26] H. Reinhardt and P. Vastag, Phys. Rev. D **94**, 105005 (2016).

[27] N. H. Christ and T. D. Lee, Phys. Rev. D **22**, 939 (1980).

[28] N. Weiss, Phys. Rev. D **24**, 475 (1981).

[29] D. Epple, H. Reinhardt, W. Schleifenbaum, and A. P. Szczepaniak, Phys. Rev. D **77**, 085007 (2008).

[30] G. Burgio, M. Quandt, and H. Reinhardt, Phys. Rev. Lett. **102**, 032002 (2009).

[31] H. Reinhardt and D. Epple, Phys. Rev. D **76**, 065015 (2007).

[32] M. Quandt and H. Reinhardt, Phys. Rev. D **96**, 054029 (2017).

[33] M. Quandt, E. Ebadati, H. Reinhardt, and P. Vastag, Phys. Rev. D **98**, 034012 (2018).

[34] C. S. Fischer, Phys. Rev. Lett. **103**, 052003 (2009).

[35] C. S. Fischer and J. A. Müller, Phys. Rev. D **80**, 074029 (2009).

[36] C. S. Fischer, A. Maas, and J. A. Müller, Eur. Phys. J. C **68**, 165 (2010).

[37] M. Quandt and H. Reinhardt, Phys. Rev. D **94**, 065015 (2016).

[38] F. E. Canfora, D. Dudal, I. F. Justo, P. Pais, L. Rosa, and D. Vercauteren, Eur. Phys. J. C **75**, 326 (2015).